NASA TECHNICAL MEMORANDUM

NASA TM X-2655

NASA TM X-2655

FLIGHT INVESTIGATION OF AN UNDERWING NACELLE INSTALLATION OF AN AUXILIARY-INLET EJECTOR NOZZLE WITH A CLAMSHELL FLOW DIVERTER FROM MACH 0.6 TO 1.3

by Verlon L. Head

Lewis Research Center
Cleveland, Ohio 44135

NATIONAL AERONAUTICS AND SPACE ADMINISTRATION • WASHINGTON, D. C. • NOVEMBER 1972

1. Report No.	2. Government Accession No.	3. Recipient's Catalog No.
NASA TM X-2655		

4. Title and Subtitle	5. Report Date
FLIGHT INVESTIGATION OF AN UNDERWING NACELLE INSTALLATION OF AN AUXILIARY-INLET EJECTOR NOZZLE WITH A CLAMSHELL FLOW DIVERTER FROM MACH 0.6 TO 1.3	November 1972
	6. Performing Organization Code

7. Author(s)	8. Performing Organization Report No.
Verlon L. Head	E-7042
	10. Work Unit No.
	764-74

9. Performing Organization Name and Address	11. Contract or Grant No.
Lewis Research Center National Aeronautics and Space Administration Cleveland, Ohio 44135	
	13. Type of Report and Period Covered
	Technical Memorandum

12. Sponsoring Agency Name and Address	14. Sponsoring Agency Code
National Aeronautics and Space Administration Washington, D.C. 20546	

15. Supplementary Notes

16. Abstract

A nozzle installation of general interest is a podded engine mounted near the aft lower surface of the wing. The effect of this installation on the performance of an auxiliary-inlet ejector nozzle with a clamshell flow diverter was investigated over a Mach number range of 0.6 to 1.3 by using a modified F-106B aircraft. The clamshell flow diverter was tested in a 17° position with double-hinged synchronized floating doors. The ejector nozzle trailing-edge flaps were simulated in the closed position with a rigid structure which provided a boattail angle of 10°. Primary nozzle area was varied as exhaust gas temperature was varied between 975 and 1561 K (1755° and 2810° R). With the nozzle in a subsonic cruise position, the nozzle gross thrust coefficient was 0.918 at a flight Mach number of 0.9.

17. Key Words (Suggested by Author(s))	18. Distribution Statement
Airframe installation effects Propulsion system Auxiliary inlet ejector Clamshell flow diverter	Unclassified - unlimited

19. Security Classif. (of this report)	20. Security Classif. (of this page)	21. No. of Pages	22. Price*
Unclassified	Unclassified	38	$3.00

* For sale by the National Technical Information Service, Springfield, Virginia 22151

FLIGHT INVESTIGATION OF AN UNDERWING NACELLE INSTALLATION OF AN AUXILIARY-INLET EJECTOR NOZZLE WITH A CLAMSHELL FLOW DIVERTER FROM MACH 0.6 TO 1.3

by Verlon L. Head

Lewis Research Center

SUMMARY

A flight test program was conducted using a modified F-106B aircraft with underwing engine nacelles to investigate airframe installation effects on an auxiliary-inlet ejector nozzle with a clamshell flow diverter over a Mach number range of 0.6 to 1.3. The clamshell flow diverter was tested in a 17° position, and only double-hinged synchronized floating doors were used. The ejector nozzle trailing-edge flaps were simulated in the closed position with a rigid structure which provided a boattail angle of 10°. Data were obtained over a range of secondary weight flows and diameter ratios of 1.74, 1.59, and 1.50, which resulted in an exhaust gas temperature variation of 975 to 1561 K (1755° to 2810° R).

Comparing installed flight performance with isolated cold-flow nozzle efficiency at the same average auxiliary door position and a subsonic cruise configuration ($d_9/d_{e8} = 1.59$) indicates that the installed flight performance is higher for subsonic Mach numbers. Compared with the plain auxiliary-inlet nozzle, the clamshell nozzle has lower performance, apparently due to the additional drag associated with adding the clamshell flow diverter.

INTRODUCTION

In its current program in airbreathing propulsion, the Lewis Research Center is investigating airframe installation effects on the performance of exhaust nozzle concepts appropriate for use at supersonic speeds. The local flow field approaching an installed nozzle may vary from isolated test conditions, thereby affecting nozzle performance (ref. 1). With an engine nacelle installation typical of a supersonic cruise aircraft, the

nacelle may be installed close to the lower surface of a large wing, with the nozzle extending downstream of the wing trailing edge. This aft location of the nacelle provides shielding of the inlet by the forward wing surface to minimize angle-of-attack effects and may also provide favorable interference effects between the wing and nacelle flow fields.

Flight data have been taken for various configurations of the variable-flap ejector, plug nozzle, and auxiliary-inlet ejector (refs. 2 to 5). From these tests, various installation effects which are both favorable and unfavorable have been found. With a nozzle type such as an auxiliary-inlet ejector, the auxiliary inlets are designed to admit tertiary air from the free stream to prevent excessive overexpansion of the primary and secondary streams at low pressure ratios. This nozzle type has the potential for being lighter than more complex variable-geometry designs (ref. 6). This weight reduction results from the use of self-actuation for both the auxiliary-inlet doors and the trailing-edge flaps, which are positioned by the pressure differential across them. The effect of nacelle installation on the local flow field can affect the nozzle by changing the tertiary-air inlet conditions and the external pressure drag. As an aircraft accelerates through the transonic speed range, the nozzle tertiary doors may close prematurely or the trailing-edge flaps may open too early giving too large an exit area, thereby producing overexpansion losses. A variation in boundary-layer height and profile can also affect the tertiary flow and, therefore, the internal performance.

The auxiliary-inlet ejector with a clamshell flow diverter investigated for this report was similar to the plain auxiliary-inlet ejector nozzle described in reference 5. It used the same floating-door hardware, and the doors were located in the same position relative to the primary nozzle as with the palin auxiliary-inlet nozzle. The clamshell provides the blockage necessary for reverse-thrust operation when it is rotated to the fully closed position. In the fully open (or supersonic cruise) position, the clamshell is intended to provide a conical expansion surface for efficient high-pressure-ratio operation. In the partly closed (or subsonic cruise) position, the secondary throat area is increased and additional flow area is provided for the tertiary flow around the outside of the clamshell.

This nozzle was previously tested in a static test facility (ref. 7) with various fixed tertiary-door positions. The purpose of the present investigation was to determine its flight performance and compare it with results of an isolated cold-flow model tested in the 8- by 6-Foot Supersonic Wind Tunnel (ref. 8). The podded engine nacelle was tangent to the wing lower surface at the trailing edge, with the nozzle extending beyond the wing approximately 1 nacelle diameter. A wing cutout area was provided so that the top three auxiliary doors opened to the flow from over the top of the wing. Only synchronized floating doors were tested; these doors simulated single-hinged trailing flaps in the

the closed position, which resulted in a 10° boattail angle. The clamshell was fixed in a position which simulated a subsonic cruise condition.

The nozzle was mounted behind a previously calibrated J85-GE-13 afterburning turbojet engine (ref. 9). The secondary air, which was required for cooling of the engine and the primary leaves, was taken from the nacelle inlet. The engine was operated over a range of power settings which resulted in primary exhaust temperature variation from 975 to 1561 K (1755° to 2810° R) and diameter ratios d_9/d_{e8} of 1.74, 1.59, and 1.50. The effect of corrected-secondary-weight-flow ratio on performance was also investigated. The nozzle was flight tested over a Mach number range of 0.6 to 1.3 and an altitude range of 4572 to 7620 meters (15 000 to 25 000 ft).

APPARATUS AND PROCEDURE

Flight Installation

Flight tests for this research program were conducted with an F-106B aircraft modified to carry two underwing nacelles, which provides a test facility for investigating nozzle and inlet concepts. The aircraft in flight is shown in figure 1 with the auxiliary-inlet ejector nozzle installed on the left nacelle. The 63.5-centimeter (25-in.) diameter nacelles were located at approximately 32-percent semispan, with the exhaust nozzles extending beyond the wing trailing edge. More details of the basic aircraft dimensions and nacelle details are given in reference 2. For this test the fixed elevon cutout section was modified to form a trough to feed air from over the wing into the top three auxiliary-door openings. Also, a wide nacelle strut, which faired back into the trough, was used. Details of the nacelle strut are also given in reference 2. A schematic drawing of the nacelle-engine installation is shown in figure 2, along with the nacelle station designations. The nacelle had a normal shock pitot inlet and contained a calibrated J85-GE-13 afterburning turbojet engine. Secondary air to cool the engine and the afterburner was supplied to the nozzle through a conical rotating valve located at the periphery of the compressor face. Secondary flow was directed underneath the nozzle housing ring to assure cooling of the primary nozzle leaves (fig. 2).

The nacelle support system consisted of a front link, a rear link, and a load-cell assembly located between the links. The nacelle axial force was transmitted to the wing through the load cell, whose axis was parallel to that of the nacelle. An accelerometer in the nacelle allowed the load cell to be compensated for axial acceleration. The axial force transmitted to the compensated load cell can be divided into two parts: (1) nacelle drag forward of the research nozzle, referred to as the tare force; and (2) research-

nozzle gross thrust minus drag. The tare force was determined from previous research test data obtained by using a calibrated cylindrical ejector nozzle (ref. 10). The research-nozzle gross thrust minus drag was determined by adding the tare force to the compensated load-cell measurement.

Primary Nozzle

The variable-area primary exhaust nozzle is made up of overlapping leaves that provide a nearly circular throat area. The leaves translate on a roller-track-cage arrangement, causing a change in the nozzle convergence angle and the location of the exit plane (fig. 3). Nozzle stations are measured from the leading edge of the nacelle inlet.

Auxiliary-Inlet Clamshell Nozzle

A side view of the ejector nozzle showing its installation relative to the trailing edge of the wing and the cover plate blocking off the door at 270° is given in figure 4. The internal geometry of the nozzle with the clamshell flow diverter in a 17° position and the J-85 variable primary nozzle closed to its minimum-area position is shown in figure 5.

The ejector trailing-edge flaps, which were simulated in the closed position, provided a boattail angle of 10° and a small radius at the boattail juncture of 0.04 nozzle diameter of 52.58 centimeters (20.7 in.), and the remaining dimensions are as shown in figure 6. The primary nozzle housing had a series of 24 rectangular holes located circumferentially around the ring. These holes were covered by a metal band so that the secondary cooling air stayed under the nozzle housing and passed over the primary leaves. The secondary flow deflector had to be positioned ahead of the holes to avoid interfering with the floating doors.

Details and dimensions of the elevon trough are given in figure 7. Figure 7(a) shows a view of the elevon trough and its position relative to the three auxiliary inlets to which it channeled the air that flowed from over the wing.

The ejector nozzle incorporated a series of 16 auxiliary inlets located around the periphery of the external skin ahead of the primary nozzle exit. Details of the double-hinged floating doors mounted in these inlets are shown in figure 8. The two doors on the sides were blocked to simulate space required for clamshell actuating mechanisms. The doors were allowed to float under the influence of air loads but were synchronized together by means of a spring clip fixture linking each door together. The doors have a 2-to-1 ratio between the aft and forward ramp angles, with the forward and aft door

ramps the same length. Each floating door had a variable-friction device consisting of spring washers and a self-locking nut (fig. 8). The doors were installed with the spring washers loose because results of a shake-table test indicated that the doors were less subject to vibration with no damping.

The principal purpose of the doors is to allow outside air to enter the ejector and to provide an aerodynamically smaller ejector exit area, which helps reduce the overexpansion of the primary jet at low values of nozzle pressure ratio. When the doors are full open (10°-20°), there is a tertiary flow area of 1052 square centimeters (163 in.^{2}); and when they are at one-half their travel (5°-10°), the flow area is 576.8 square centimeters (89.4 in.^{2}).

Instrumentation

Total pressure and temperature of the secondary air were obtained from probes located at the exit of the flow passage under the primary nozzle housing ring, as indicated in figure 2. The probes were located at circumferential positions of 0°, 90°, 180°, and 270°. The thermocouples were Chromel-Alumel and had radiation shields.

Instrumentation for the ejector nozzle body, auxiliary doors, and clamshell flow diverter is presented in figure 9. Boundary-layer rakes were positioned both upstream and downstream of the auxiliary doors at the three circumferential positions shown in figure 9(a). Also shown in figure 9(a) are the five tertiary total-pressure rakes located just downstream of the door trailing edge. Each of the same five doors has a row of equally spaced external static-pressure orifices located along the door centerline, with their locations given in figure 9(b). The static pressures acting on the internal surface of the doors were obtained from orifices located on the inside surface of four of the struts between doors, as shown in figure 9(c). All the floating doors, except the two blocked ones, were instrumented to record door position with the use of potentiometers. The external static-pressure orifices on the ejector nozzle are shown in figure 9(d). Three rows of static-pressure orifices were located on the cylindrical section upstream of the doors at 0°, 135°, and 180°. Three rows of static-pressure orifices were located downstream of the doors on the cylindrical section and the boattail at 0°, 90°, and 180°. Internal static-pressure and wall-surface-temperature instrumentation on the ejector shroud is shown in figure 9(e). Four rows of static-pressure orifices were located at 0°, 45°, 90°, and 180°. One row of wall-surface-temperature sensors were located at 90°, plus additional single ones at 0°, 180°, and 270° near the shroud trailing edge. Static-pressure and surface-temperature instrumentation on the clamshell flow diverter is shown in figure 9(f). Both the inside and outside surfaces were instrumented with

static-pressure orifices in order to calculate drag. Only the inside surfaces were instrumented to obtain surface temperatures.

An onboard digital data system was used to record the pressures and temperatures on magnetic tape. It had the capability of recording 578 parameters in 11.52 seconds (ref. 10). There was also a 14-channel onboard analog data system. Positions of all the doors were recorded on the digital system, and five door positions were also recorded on the analog system to study their dynamic behavior.

A flight-calibrated test boom located on the aircraft nose was used to determine the free-stream static and total pressures, aircraft angle of attack, and yaw angle.

APPARATUS AND PROCEDURE

Procedure

Performance characteristics of the ejector nozzle were obtained over flight Mach numbers from 0.6 to 1.3 and at Reynolds numbers that varied from 8.5×10^6 per meter (2.6×10^6/ft) at Mach 0.6, to 14×10^6 per meter (4.4×10^6/ft) at Mach 1.3. The aircraft was flown at the nominal altitude - Mach number profile shown in figure 10(a), which resulted in the angles of attack and elevon deflection shown in figure 10(b). The exhaust nozzle pressure ratio schedule is given in figure 10(c) as a function of Mach number. Three power settings were investigated and the resulting values of primary nozzle effective area A_{e8} and corresponding values of diameter ratio d_9/d_{e8}, exhaust gas temperature T_8, and corrected-secondary-weight-flow ratio $\omega\sqrt{\tau}$ are given in table I.

Data Reduction

Engine airflow was determined by using the calibration results from reference 9, along with measurements of engine speed and total pressure and temperature at the compressor face. Fuel flows were obtained from calibrated flow meters. Total temperature T_8, total pressure P_8, and effective area A_{e8} were obtained by using the values of engine airflow and fuel flow, the measured values of total pressure and temperature at the turbine discharge (station 5), and afterburner temperature rise and pressure drop calibration results from reference 9.

Three different performance parameters are presented. The first, nozzle efficiency, is defined as ejector nozzle gross thrust minus drag divided by the sum of the ideal trhust of the primary and secondary streams:

$$\frac{F - D}{F_{ip} + F_{is}}$$

The second performance parameter, gross thrust coefficient, is similar to the first except the gross thrust minus drag is divided by only the ideal thrust of the primary stream:

$$\frac{F - D}{F_{ip}}$$

The third parameter, internal performance coefficient, excludes the external forces on the nozzle:

$$\frac{F - D}{F_{ip}} + \frac{D_\beta + D_f + D_{aux}}{F_{ip}}$$

The ideal thrust of the primary stream F_{ip} was determined from the calculated primary mass flow expanded isentropically to ambient pressure from its value of total pressure and temperature at station 8 (primary exit). The drag is the sum of the pressure drag on the boattail and auxiliary doors and the skin-friction drag. Skin-friction calculations were based on an equivalent wetted area of a flat plate and an average Reynolds number. Pressure drags were obtained by assigning to each pressure orifice an incremental area projected on a plane normal to the nozzle axis and summing the incremental forces. For the boattail, the drag force was calculated as follows:

$$D_\beta = \left\{ p_o - \left[\frac{1}{4} \frac{\left(\sum p_{13\text{-}21} \right)_{0^o}}{9} + \frac{1}{2} \frac{\left(\sum p_{13\text{-}21} \right)_{90^o}}{9} + \frac{1}{4} \frac{\left(\sum p_{13\text{-}21} \right)_{180^o}}{9} \right] \right\} A_\beta$$

The 270^o quadrant is assumed to have the same pressure distribution as the 90^o quadrant is weighted twice as much as the 0^o and 180^o quadrants. The auxiliary-inlet-door drag was calculated by using the following equation:

$$D_{aux} = \left[p_o - \left(\frac{1}{16} \frac{\overbrace{\sum p_{4-6} \cos \nu_u + p_{7-9} \cos \nu_d}^{\text{Door 1}}}{6} + \frac{1}{8} \frac{\overbrace{\sum p_{4-6} \cos \nu_u + p_{7-9} \cos \nu_d}^{\text{Door 2}}}{6} \right.\right.$$

$$+ \frac{1}{8} \frac{\overbrace{\sum p_{4-6} \cos \nu_u + p_{7-9} \cos \nu_d}^{\text{Door 3}}}{6} + \frac{3}{8} \frac{\overbrace{\sum p_{4-6} \cos \nu_u + p_{7-9} \cos \nu_d}^{\text{Door 7}}}{6}$$

$$\left.\left. + \frac{5}{16} \frac{\overbrace{\sum p_{4-6} \cos \nu_u + p_{7-9} \cos \nu_d}^{\text{Door 9}}}{6} \right) \right] A_{aux}$$

Each static-pressure orifice on the doors was located in the center of equal areas and the door area A_{aux} is the total surface area of the 16 doors. The five instrumented doors (1, 2, 3, 7, and 9) were considered typical for various numbers of uninstrumented doors which determined the weighting factors used in the preceding equation. The static-pressure orifice numbers in the preceding two equations correspond to the locations shown in figure 9.

The clamshell static-pressure orifices were not located in the center of equal areas, so each orifice had its own individual area assigned to it. The drag of the clamshell is simply the difference of the sum of the pressure-area products $\left(\sum p_x A_x\right)$ for the upstream-facing surfaces and the sum of the pressure-area products $\left(\sum p_x A_x\right)$ for the downstream-facing surfaces. The drag for the internal surface of the shroud was calculated similar to the boattail drag, where each row of pressure orifices was assigned an area-weighting factor, except that within each row the individual pressure orifices did not have the same area assigned to them.

RESULTS AND DISCUSSION

The flight performance data of this investigation are compared to isolated performance data from a 21.6-centimeter (8.5-in.) diameter cold-flow model taken in the Lewis 8- by 6-Foot Supersonic Wind Tunnel (ref. 8). The isolated model did not have floating inlet doors but was tested with fixed double-hinged doors at positions of 0°, 5°-10°, 8°-16°, and 10°-20°.

A comparison of the efficiency of the installed nozzle, at minimum reheat power, with the peak efficiency of the isolated wind tunnel model shows very little difference

from Mach 0.7 to 0.98, as shown in figure 11. Comparisons are made for only the minimum-reheat power setting because this closely matches a typical subsonic cruise area ratio and pressure ratio for a supersonic cruise aircraft.

If the isolated data are interpolated for the same door position as well as for a pressure ratio that matched the flight data, the isolated nozzle efficiency is considerably lower from Mach 0.68 to 0.985. Below Mach 0.68 the isolated nozzle efficiency is slightly higher.

The clamshell ejector nozzle performance characteristics are shown in figure 12 for diameter ratios of 1.74 (nonreheat), 1.59 (minimum reheat), and 1.50 (reheat B). A comparison is made with the plain auxiliary-inlet nozzle for the minimum reheat condition (ref. 5).

The gross thrust coefficient for the installed nozzle is presented in figure 12(a) for the three power settings tested. The performance is quite low for both the military (nonreheat) and minimum-reheat power settings at all Mach numbers. Figure 12(b) shows the internal performance coefficient for the same three power settings, which again is low. The pumping characteristics are shown in figure 12(c). In all three parts of figure 12 the performance of the plain auxiliary-inlet ejector (AIE) nozzle is shown for a comparison in minimum reheat since this is close to a typical subsonic cruise area ratio. The plain AIE nozzle was similar except for the clamshell flow diverter and a 29.5-percent-larger exit area (d_9/d_{e8} of 1.40 as compared to 1.59).

The plain auxiliary-inlet nozzle had a higher gross thrust coefficient and internal performance coefficient than the AIE-clamshell nozzle at subsonic Mach numbers, as shown in figure 12(a) and (b). The largest difference was 5 percent and occurred at a flight Mach number of 0.95. At Mach numbers from 1.0 to 1.3 the AIE is only 1.5 to 2 percent higher. Figure 12(c) shows the plain AIE to be a better pumper until Mach 1.08. Above Mach 1.08 the AIE-clamshell nozzle is better since its minimum pumping pressure ratio P_s/P_8 is lower than that of the plain AIE with its smaller diameter ratio.

A breakdown of the ejector component drag is shown in figure 13. Shown in the figure are the boattail drag coefficients and ratios of boattail, auxiliary door, internal shroud, and total ejector nozzle drags to the ideal primary thrust as a function of Mach number for the three primary power settings. The trend of low and nearly constant values of boattail drag coefficient below Mach 0.95 seen from nozzle data previously obtained on the F-106 is again evident for this nozzle. It is shown in figure 13(d) that the clamshell produces a thrust for military and minimum-reheat power settings below Mach 0.95 and a drag at higher Mach numbers. In the region where a drag is produced, the clamshell could be rotated towards zero degrees to eliminate or at least reduce the drag, as indicated from the isolated data of reference 8. For the reheat B power setting, the clamshell could be rotated at all Mach numbers tested to reduce the clam-

shell drag. There were limitations to the amount of instrumentation that could be used on the clamshell, so the leading edges and the hinge-pin support area were not instrumented. If instrumented, these areas would have shown up as drag forces and reduced or possibly cancelled the thrust force calculated from the available instrumentation for Mach numbers less than 0.95 and increased the magnitude of the drag force at higher Mach numbers. It should be noted in figure 13(f) that the total drag of the ejector in the subsonic region is fairly low, which does not explain why it has a lower internal performance coefficient than the plain AIE nozzle. As already mentioned, more complete instrumentation for the clamshell would increase its drag force and possibly account for most of the difference between the two nozzles.

The effect of secondary flow on nozzle performance characteristics is shown in figure 14 for a flight Mach number of 0.9. The corrected-secondary-weight-flow ratio was varied from 0.024 to 0.073 for military and minimum reheat. For reheat B, only small variations around a value of 0.07 were obtained because of cooling requirements. The effect of increasing secondary flow was to raise the nozzle gross thrust coefficient by about 2 percent (fig. 14(a)). If the nozzle gross thrust coefficient were penalized for the ram drag of the secondary flow, there would be no noticeable change in performance.

In figure 14(b) the boattail drag ratioed to ideal primary thrust is presented as a function of secondary airflow. The results show a slight increase in drag with increasing secondary flow and a slight lowering of the flap moment coefficient, as shown in figure 14(c). Another result was that the doors floated to a more closed position because of the higher secondary pressure that was required. The variation in door position and ratio of secondary to primary total pressure as a function of secondary flow is shown in figures 14(d) and (e), respectively.

Although the floating auxiliary-inlet doors were synchronized, the linkage between doors did allow some relative movement between each door. This is illustrated in figure 15 for a minimum-reheat power setting and a flight Mach number of 0.9. Although inlet openings for doors 5 and 13 were closed off, they still affected the movement of the doors adjacent to them since the doors remained linked together. It can be seen from the figure that there is a large circumferential variation in door position.

The trailing-edge flap moment and auxiliary-inlet floating door characteristics are shown in figure 16. The average position of the 14 doors (excludes the two closed doors) is shown in figure 16(a). The door positions did not change much until Mach 0.9, then the doors became more closed - almost fully closed with the reheat B power setting. With a military or minimum-reheat power setting, as the Mach number was raised above 0.97 the doors became more open, with a peak occurring at Mach 1.05 before they became more closed again.

The flap moment coefficient presented in figure 16(b) shows that the trailing flap, if made floating, would have opened for all power settings and flight speeds except near

Mach 0.9. At Mach 0.97 the boattail drag rise begins as the shock passes over the boattail, emersing it in supersonic flow. This lowers the boattail pressures, thereby increasing the flap opening moment coefficient, which peaks at Mach 1.03. As flight Mach number is increased above 1.05 and the nozzle pressure ratio goes up, the nozzle becomes less overexpanded, thus lowering the internal wall static pressures relative to ambient. This fact, in addition to the boattail pressures increasing slightly with Mach number, lowers the opening moment on the flap for military and minimum-reheat power settings. For reheat B ($d_9/d_{e8} = 1.5$) the flap moment stays the same because the wall static pressures are increasing above Mach 1.05 to just offset the increasing boattail pressures.

Moment coefficients and door positions are shown in figure 17 for the five floating doors which had static-pressure instrumentation. Free-floating doors would normally indicate a zero moment; but with synchronized doors under the influence of a circumferential static-pressure variation such as this underwing installation produces, the doors do not always indicate a zero moment. This is shown in figure 17(a) for a minimum-reheat power setting. In figure 17(b) the same individual door positions are presented to show the wide circumferential variation in door position that exists over the Mach number range tested.

The boundary-layer velocity profiles also vary around the circumference of the nozzle ahead of the auxiliary-door openings, as shown in figure 18. The velocity profiles are presented for three angular positions at four flight Mach numbers to 0.95. The values for momentum thickness calculated from each of the profiles are also given. As can be seen from the figure, the local velocities near the surface are a lower fraction of free-stream velocity than would be expected to give good pressure recovery in the auxiliary inlets. This is confirmed by examining the results obtained from the total-pressure measurements taken at the trailing edge of five doors for a Mach number of 0.9, which are presented in figure 19.

The static-pressure distribution along the internal surface of the nozzle shroud downstream of the tertiary-door openings at a flight Mach number of 0.9 is shown in figure 20 for a minimum-reheat power setting. The tertiary doors are almost full open; and although the nozzle is still overexpanded, there must be enough tertiary air entering the doors to keep the static pressure slightly above ambient over most of the shroud internal surface. The static pressure and clamshell surface temperature distributions are shown in figure 21 for the same nozzle conditions as for figure 20. The static pressures on both the inside and outside surfaces of the clamshell are near or slightly above ambient. As expected, the peak temperature occurs at the trailing edge of the clamshell, as shown in figure 21(c).

SUMMARY OF RESULTS

A flight investigation was conducted to determine the performance of an installed auxiliary-inlet ejector nozzle with a clamshell flow diverter over a Mach number range of 0.6 to 1.3 and to compare it with isolated cold-flow results. The clamshell flow diverter was fixed in the subsonic cruise position (17°), and the trailing-edge flaps were simulated in the closed position. Only double-hinged synchronized floating doors were used.

Data were obtained over a range of secondary weight flows and diameter ratios of 1.74, 1.59, and 1.50. Results of the investigation are summarized as follows:

1. The installed flight performance is higher than the isolated cold-flow nozzle efficiency at the same average door position and a subsonic cruise configuration ($d_9/d_{e8} = 1.59$) to 0.985.

2. There is little difference between the nozzle efficiency from the flight tests and that from tests of the isolated model with a fixed door position that gave the highest efficiency.

3. Compared with the plain auxiliary-inlet nozzle, the clamshell nozzle has lower performance, apparently because of the additional drag associated with adding the clamshell flow diverter.

4. If the trailing-edge flaps had been floating rather than fixed, they would have moved off the inner stops at all Mach numbers except near 0.965, and thus the overall performance would have been lower.

5. Increasing secondary-corrected-weight-flow ratio from 0.024 to 0.070 at Mach 0.9 increased the gross thrust coefficient about 1.6 percent for the subsonic cruise configuration. However, this increase would be lost if the nozzle were penalized for the ram drag of the secondary flow.

Lewis Research Center,
National Aeronautics and Space Administration,
Cleveland, Ohio, August 3, 1972,
764-74.

APPENDIX - SYMBOLS

A	cross-sectional area (cold), cm^2 ($in.^2$)
A_n	cross-sectional area of nozzle cylindrical section, 3166.9 cm^2 (490.9 $in.^2$)
C	maximum chord length of clamshell flow diverter, 33.02 cm (13 in.)
C_{D_β}	axial boattail pressure drag coefficient in direction of nozzle axis, Axial force/ $q_0 A_n$
C_m	moment coefficient, Moment/$q_0 A_n d_n$
D	drag in direction of zero nozzle axis, kN (lbf)
d	diameter, cm (in.)
d_n	diameter of nozzle cylindrical section, 63.5 cm (25 in.)
F	nozzle thrust along nozzle axis, kN (lbf)
h	geopotential pressure altitude, m (ft)
L	distance from leading edge of clamshell flow diverter, cm (in.)
M	Mach number
P	absolute total pressure, kN/m^2 (psi)
p	absolute static pressure, kN/m^2 (psi)
q	dynamic pressure, $0.7\, p_0 M_0^2$, kN/m^2 (psi)
r	boattail juncture radius, cm (in.)
T	absolute total temperature, K (^oR)
T_w	clamshell surface temperature, K (^oR)
V	boundary-layer velocity, m/sec (ft/sec)
V_L	maximum velocity calculated in boundary layer, m/sec (ft/sec)
V_0	free-stream vellcity, m/sec (ft/sec)
W	weight flow, kg/sec (lbm/sec)
x	axial distance from primary nozzle exit, cm (in.)
x_p	primary nozzle exit location, cm (in.)
y	distance from nozzle external surface, cm (in.)
z	distance from nozzle shroud internal surface, cm (in.)

α_0	aircraft angle of attack, deg
α_p	primary nozzle convergence angle, deg
β	boattail angle, deg
δ_e	elevon deflection (+ down, - up), deg
δ^{**}	boundary-layer momentum thickness, cm (in.)
ν	auxiliary-inlet-door ramp angle, deg
φ	angular position (looking upstream), deg
τ	ratio of secondary to primary total temperatures at station 8
ω	ratio of secondary to primary weight flows at station 8
$\omega\sqrt{\tau}$	corrected-secondary-weight-flow ratio

Subscripts:

aux	auxiliary-inlet door
clm	clamshell flow diverter
d	downstream auxiliary door ramp
e	effective
ext	external nozzle surface including auxiliary doors
F	trailing-edge flap
f	aerodynamic skin friction
ip	ideal primary
is	ideal secondary
n	nozzle
p	primary
SI	shroud internal surface
s	secondary
T	total shroud plus flow-diverter surfaces
ter	tertiary
u	upstream auxiliary door ramp
w	internal shroud wall surface
0	free stream
1-9	nacelle and nozzle stations (see fig. 2)

REFERENCES

1. Nichols, Mark R.: Aerodynamics of Airframe - Engine Integration of Supersonic Aircraft. NASA TN D-3390, 1966.

2. Mikkelson, Daniel C.; and Head, Verlon L.: Flight Investigation of Airframe Installation Effects on a Variable Flap Ejector Nozzle of an Underwing Engine Nacelle at Mach Numbers From 0.5 to 1.3. NASA TM X-2010, 1970.

3. Head, Verlon L.: Flight Investigation of an Underwing Nacelle Installation of Three Variable-Flap Ejector Nozzles. NASA TM X-2478, 1972.

4. Samanich, Nick E.; and Chamberlin, Roger: Flight Investigation of Installation Effects on a Plug Nozzle Installed on an Underwing Nacelle. TM X-2295, 1971.

5. Burley, Richard R.: Flight Investigation of Airframe Installation Effects on an Auxiliary Inlet Ejector Nozzle on an Underwing Engine Nacelle. NASA TM X-2396, 1971.

6. Migdal, David; and Horgan, John J.: Thrust Nozzles for Supersonic Transport Aircraft. J. Eng. Power, vol. 86, no. 2, Apr. 1964, pp. 97-104.

7. Mansour, Ali H.; and Burley, Richard R.: Internal Thrust and Pumping Performance of an Auxiliary Inlet Ejector Nozzle with Clamshell Thrust Reverser. NASA TM X-52621, 1969.

8. Steffen, Fred W.; and Johns, Albert L.: Performance of a Fixed Geometry Wind Tunnel Model of an Auxiliary Inlet Ejector with a Clamshell Flow Diverter from Mach 0 to 1.2. NASA TM X-2037, 1970.

9. Antl, Robert J.; and Burley, Richard R.: Steady-State Airflow and Afterburning Performance Characteristics of Four J85-GE-13 Turbojet Engines. NASA TM X-1742, 1969.

10. Groth, Harold W.; Samanich, Nick E.; and Blumenthal, Philip Z.: Inflight Thrust Measuring System for Underwing Nacelles Installed on a Modified F-106 Aircraft. NASA TM X-2356, 1971.

TABLE I. - ENGINE POWER SETTINGS

J85 power setting	Nozzle throat effective area, A_{e8}		Nominal ratio of ejector exit diameter to primary nozzle effective diameter, d_9/d_{e8}	Nozzle throat total temperature, T_8		Corrected-secondary-weight-flow ratio, $\omega\sqrt{\tau}$
	cm^2	$in.^2$		K	^oR	
Nonreheat (military)	695 to 732	107 to 113	1.74	975 to 999	1755 to 1799	0.025 to 0.073
Minimum reheat	849 to 878	132 to 136	1.59	1221 to 1313	2197 to 2363	.024 to .072
Reheat B	930 to 964	144 to 149	1.50	1413 to 1561	2543 to 2810	.066 to .074

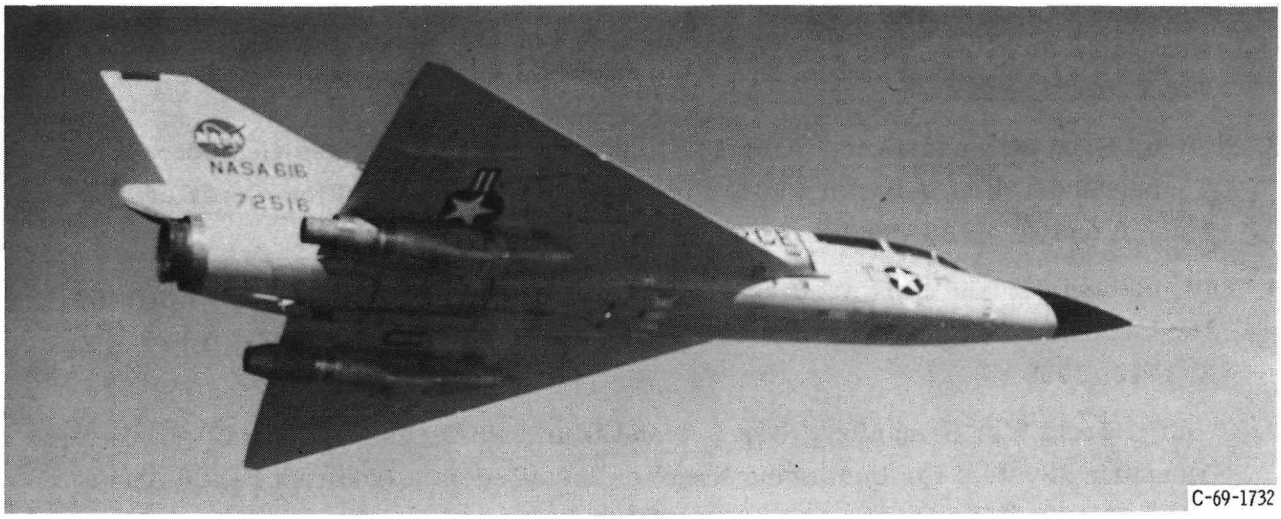

Figure 1. - Modified F-106B aircraft in flight, showing underwing installation of nozzles.

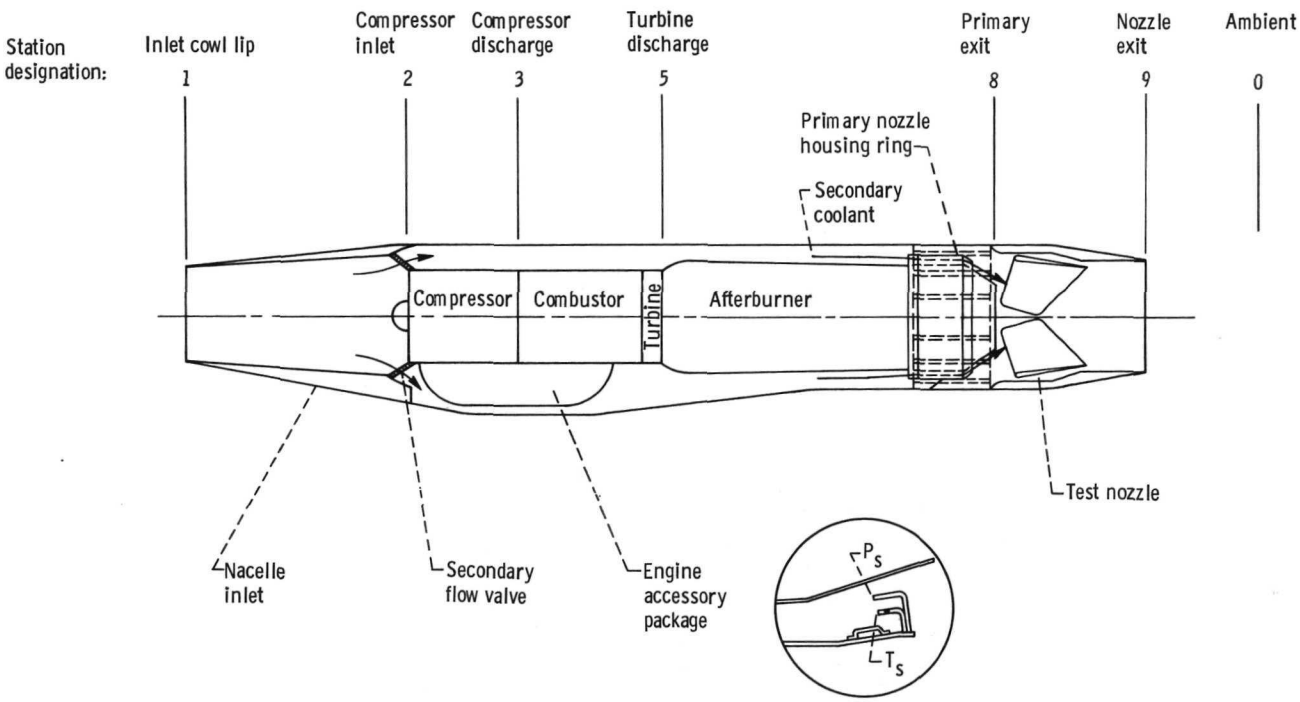

Figure 2. - Schematic of nacelle-engine installation and station designation.

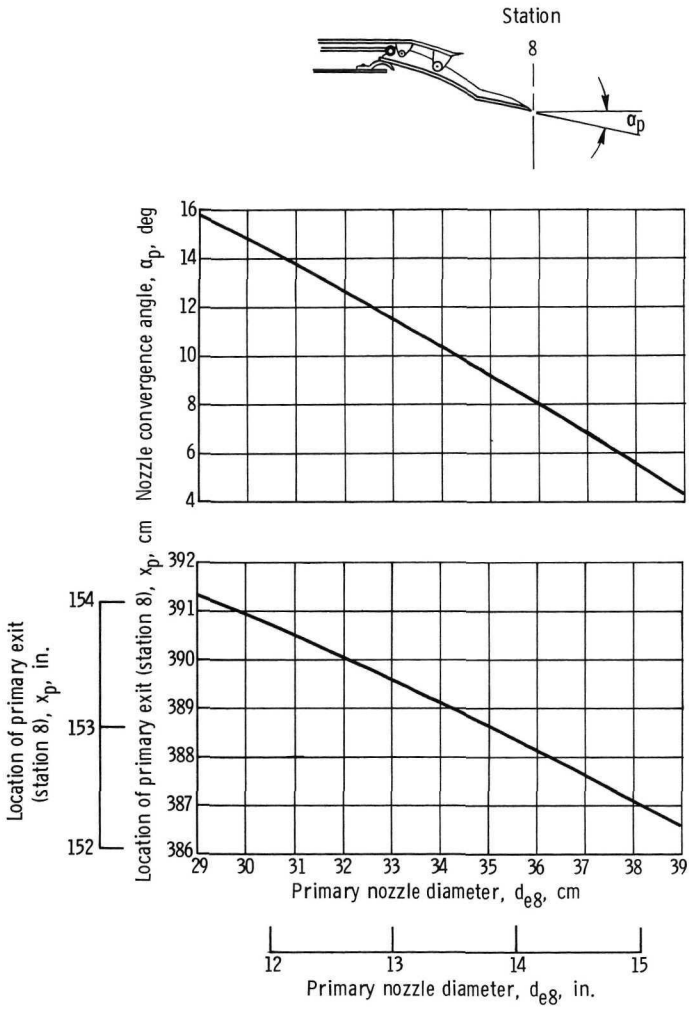

Figure 3. - Location of primary nozzle exit plane and nozzle convergence angle variation.

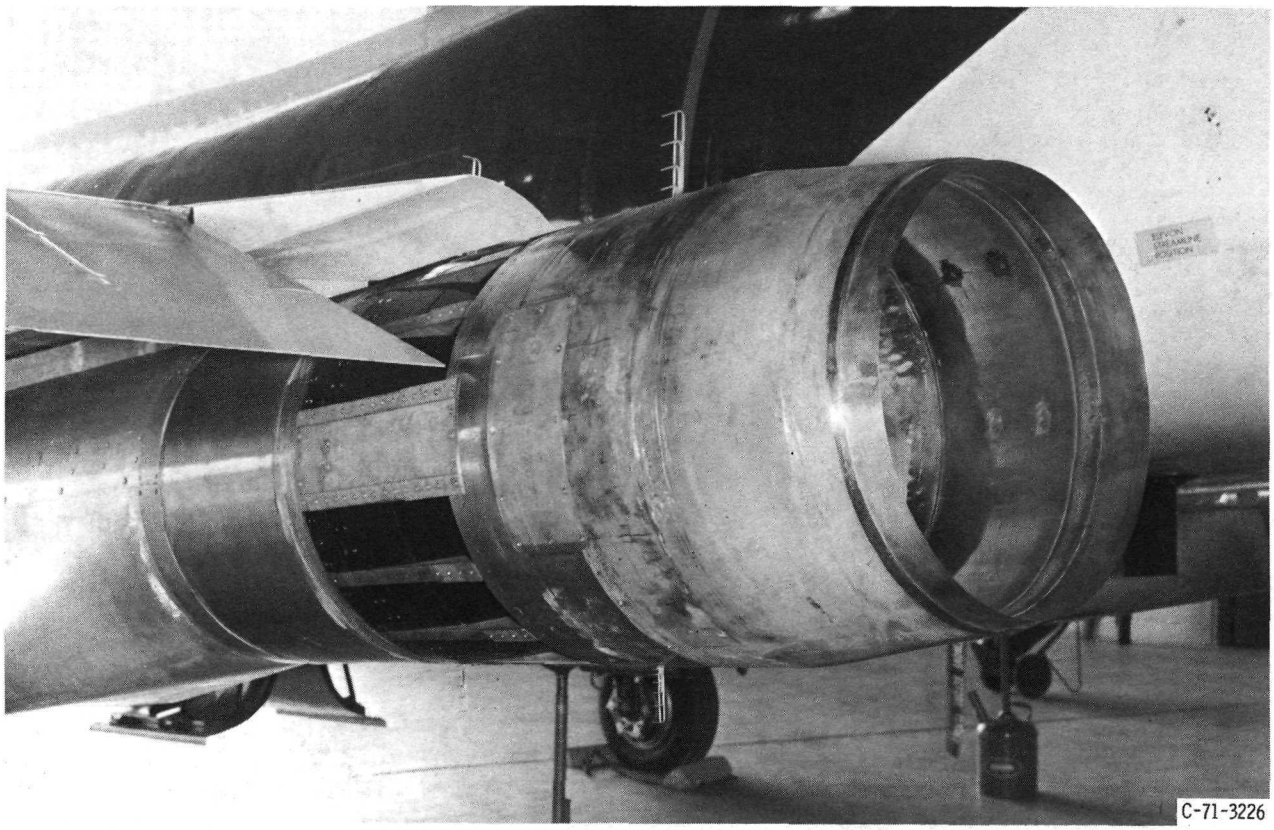

Figure 4. - Auxiliary-inlet ejector nozzle with clamshell flow diverter located under trailing edge of wing.

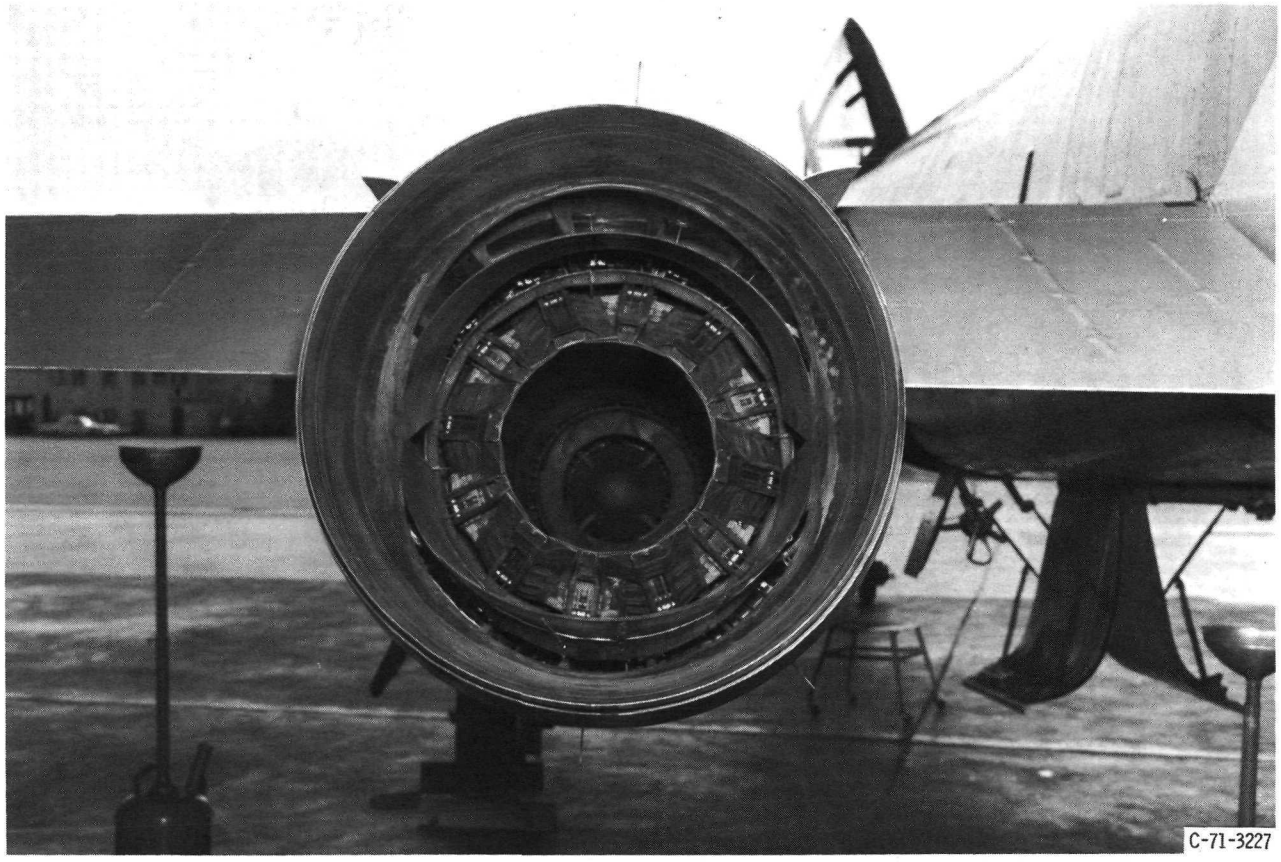

Figure 5. - Internal geometry of ejector nozzle, showing clamshell flow diverter in a 17^{0} position and primary variable nozzle in minimum-area position (nonreheat, $d_9/d_{e8} = 1.74$).

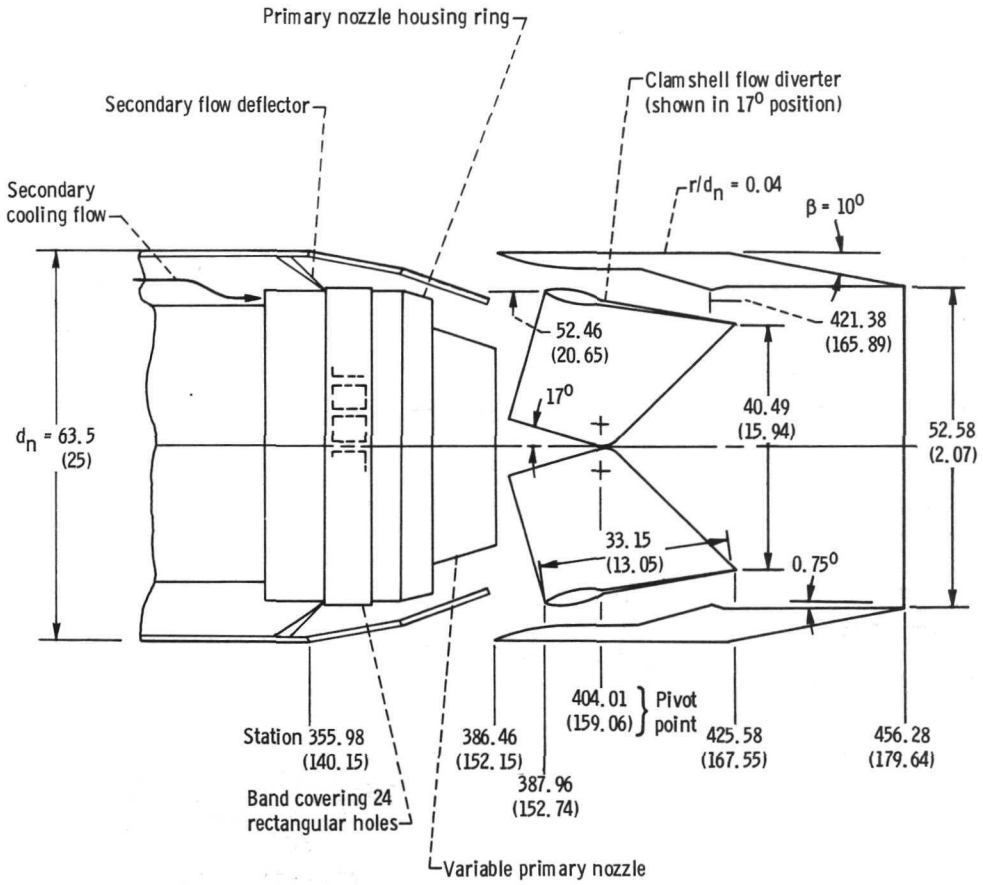

Figure 6. - Dimensional characteristics of ejector nozzle. (All dimensions are in cm (in.).)

(a) Faired elevon trough, showing its location relative to wing with the elevons deflected down and auxiliary-inlet doors.

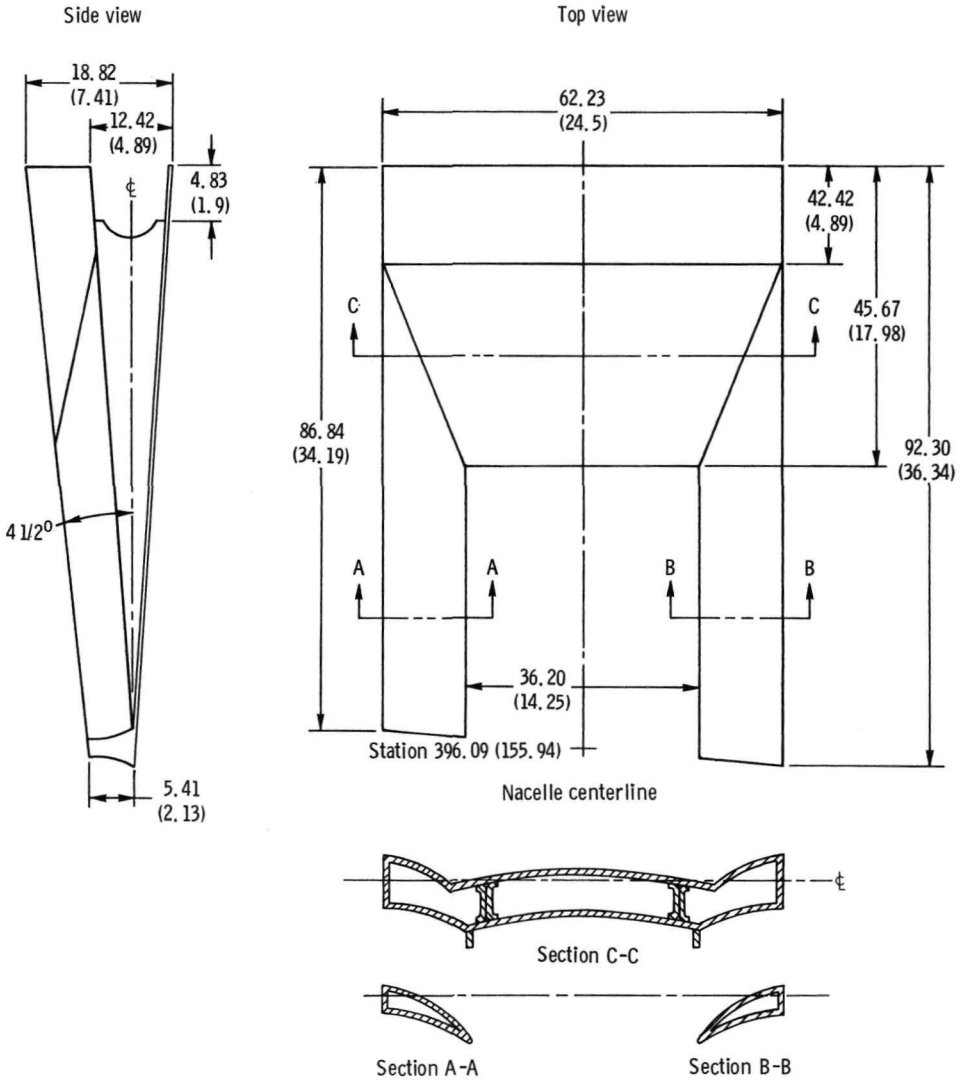

(b) Elevon trough.

Figure 7. - Details of elevon trough.

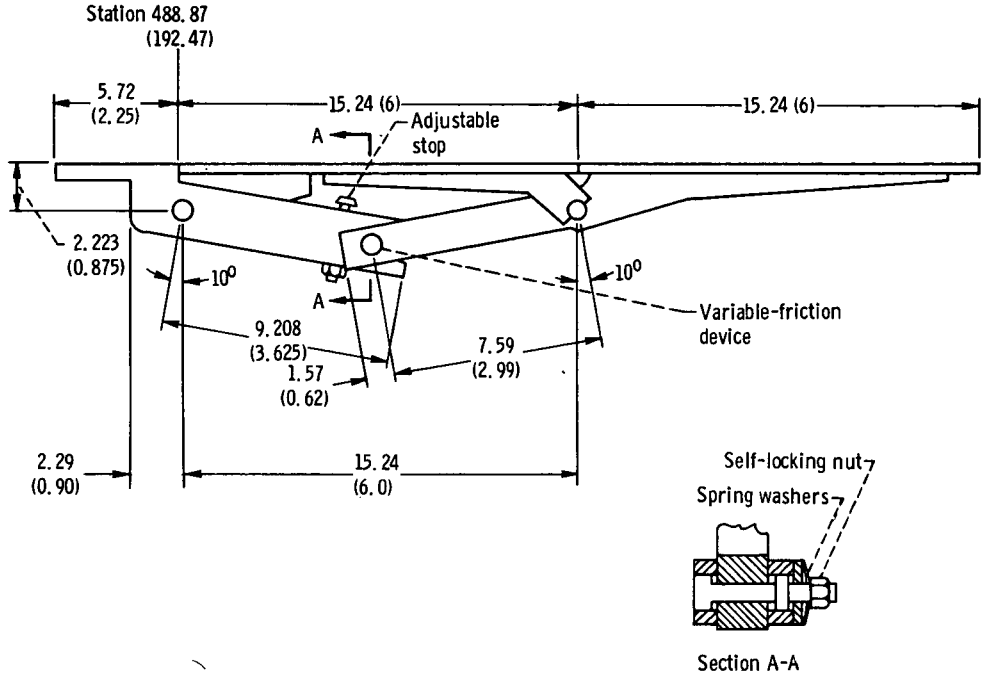

Figure 8. - Dimensional characteristics of floating auxiliary-inlet doors. Door width, 9.83 centimeters (3.87 in.).

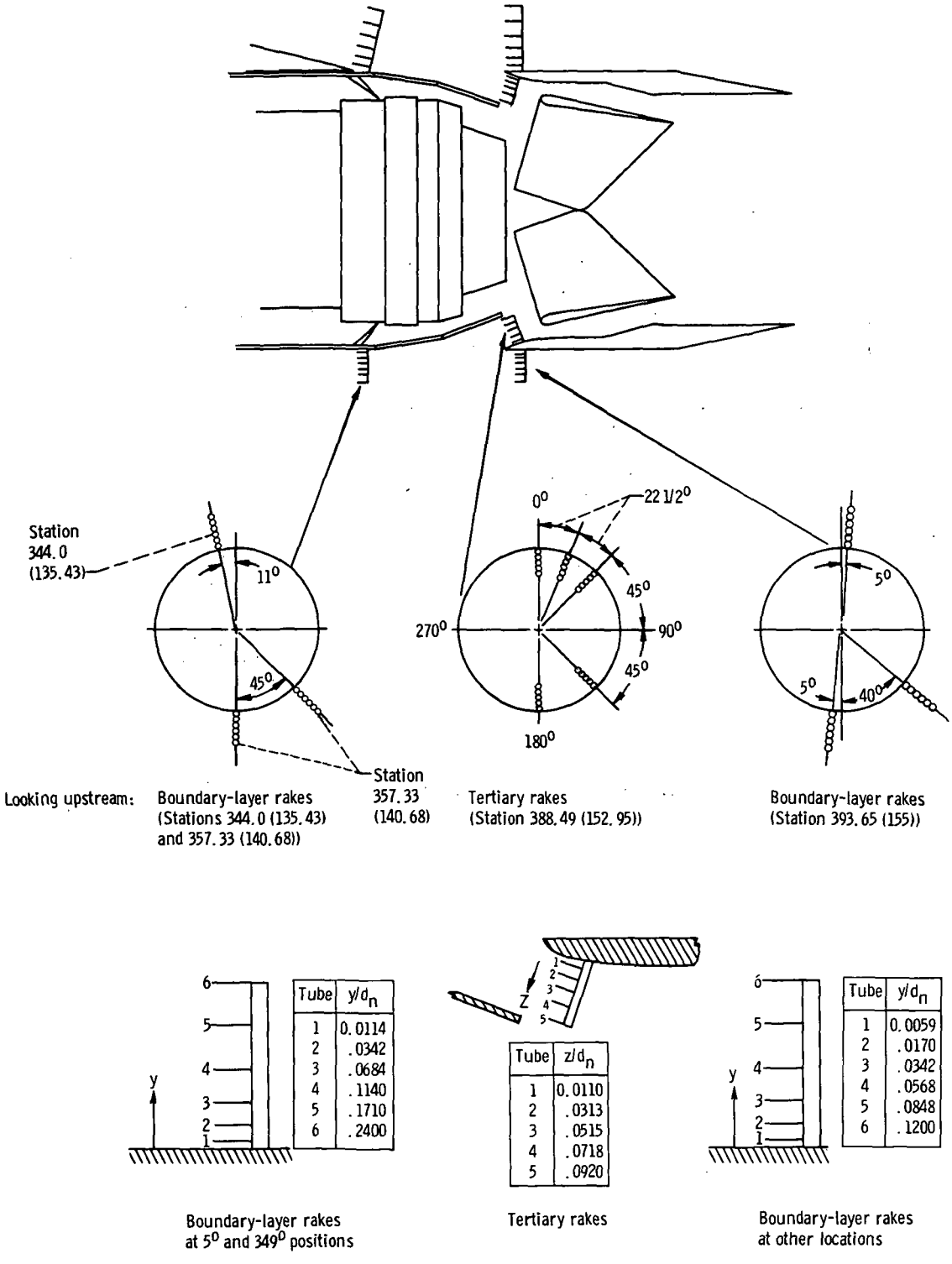

(a) Boundary-layer and tertiary rakes.

Figure 9. - Ejector nozzle instrumentation details.

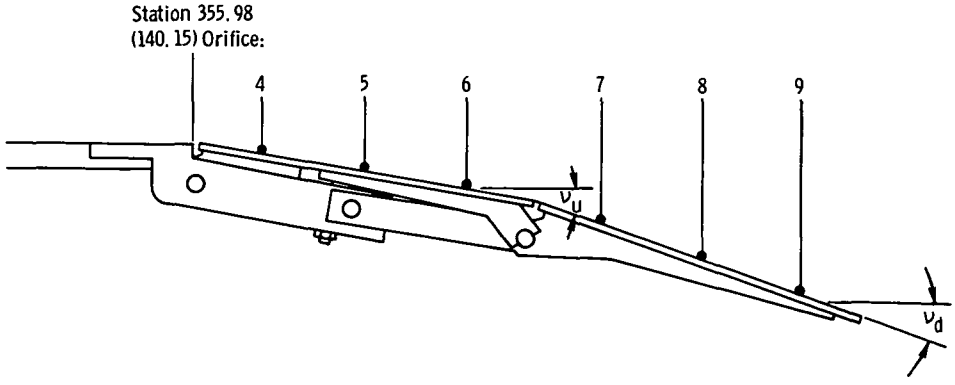

Orifice	Door position, deg					
	$\nu_u = \nu_d = 0^0$		$\nu_u = 5^0$, $\nu_d = 10^0$		$\nu_u = 10^0$, $\nu_d = 20^0$	
	Station					
	cm	in.	cm	in.	cm	in.
4	358.52	141.15	358.50	141.14	358.47	141.13
5	363.55	143.13	363.52	143.12	358.39	141.10
6	368.55	145.10	368.53	145.09	368.53	145.09
7	373.50	147.05	373.58	147.08	373.38	147.00
8	378.41	148.98	378.33	148.95	378.13	148.87
9	383.29	150.90	383.21	150.87	382.98	150.78

(b) Auxiliary-inlet-door external static pressures. Circumferential location of instrumented doors: 0^0, 22 1/2, 45^0, 135^0, 180^0 (looking upstream).

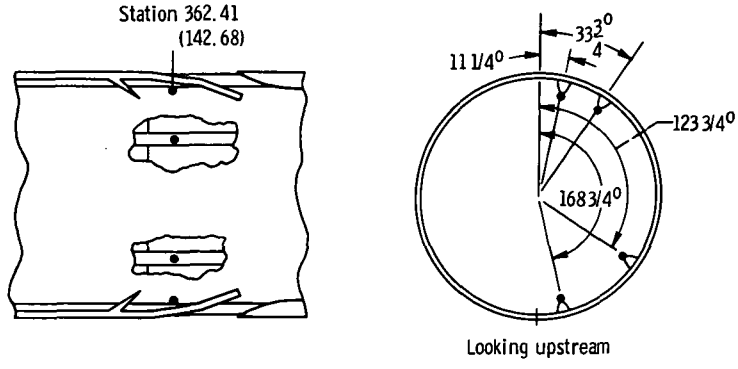

(c) Auxiliary-inlet-door internal static-pressure orifices.

Figure 9. - Continued.

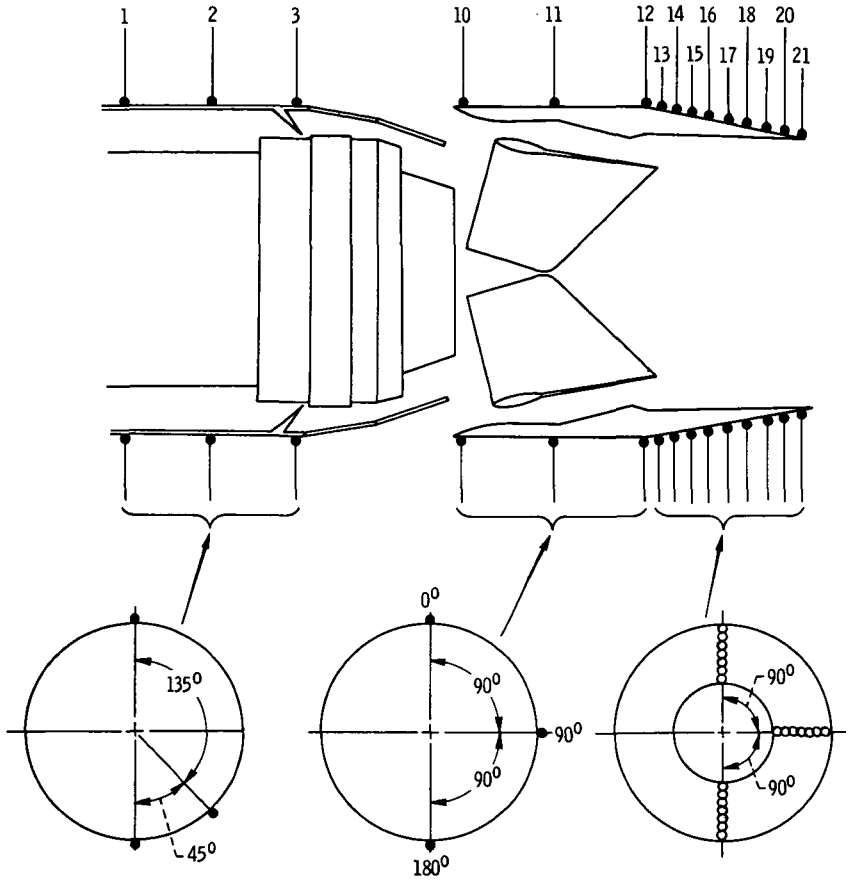

Looking upstream

Orifice	Station	
	cm	in.
1	322.73	127.06
2	339.44	133.64
3	355.98	140.15
10	387.09	152.40
11	405.26	159.55
12	424.05	166.95
13	425.63	167.57
14	428.98	168.89

Orifice	Station	
	cm	in.
15	432.43	170.25
16	435.91	171.62
17	439.42	173.00
18	443.00	174.41
19	446.76	175.89
20	450.44	177.34
21	454.38	178.89

(d) External static-pressure orifices.

Figure 9. - Continued.

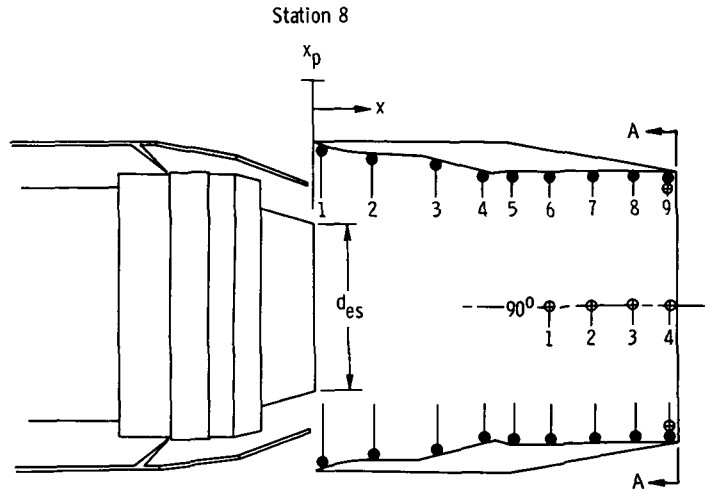

Static-pressure orifice	Station	
	cm	in.
1	388.49	152.95
2	397.87	156.64
3	409.55	161.24
4	419.71	165.24
5	424.79	167.24
6	432.66	170.34
7	440.54	173.44
8	448.41	176.54
9	455.65	179.39

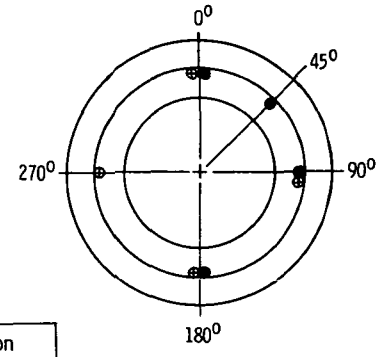

Section A-A
(looking upstream)

Wall temperature instrumentation	Station	
	cm	in.
1	432.66	170.34
2	440.54	173.44
3	448.41	176.54
4	455.65	179.39

(e) Internal static-pressure and wall-temperature instrumentation.
(x = Station - x_p, $x_p = f(d_{e8})$ (see fig. 3).)

Figure 9. - Continued.

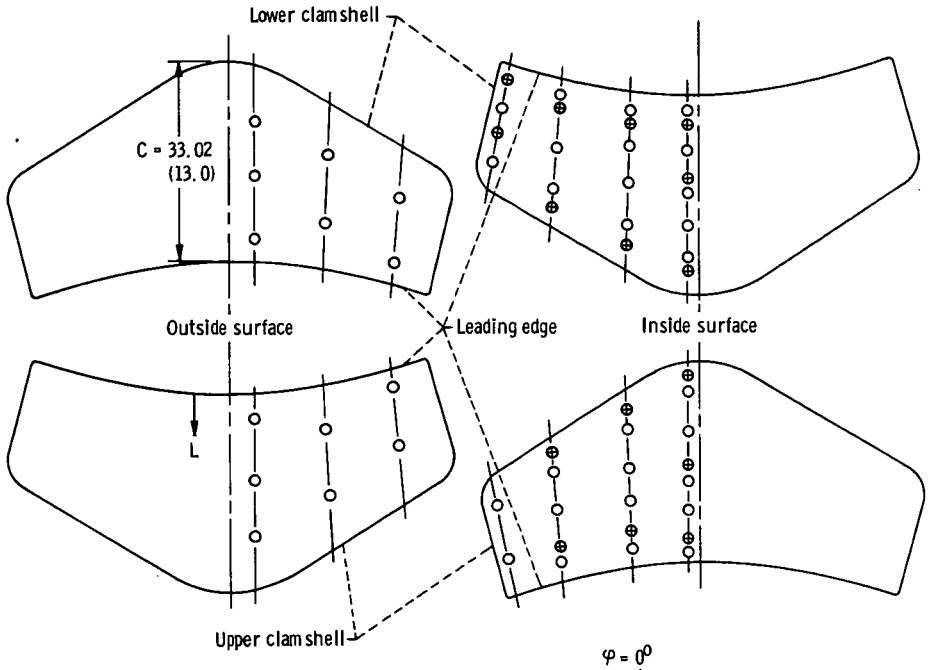

Static pressures

Angular position, φ	L/C	Distance from leading edge, L	
		cm	in.
Inside surface			
5^0, 175^0	0.096	3.175	1.25
	.287	9.525	3.75
	.479	15.875	6.25
	.670	22.225	8.75
	.862	28.575	11.25
31^0, 149^0	0.096	3.175	1.25
	.328	10.874	4.28
	.560	18.572	7.31
	.793	26.271	10.34
59^0, 121^0	0.096	3.175	1.25
	.371	12.294	4.84
	.646	21.412	8.43
86^0, 94^0	0.096	3.175	1.25
	.326	10.795	4.25
Outside surface			
194^0, 346^0	0.153	5.080	2.00
	.460	15.240	6.00
	.766	25.400	10.00
220^0, 320^0	0.153	5.080	2.00
	.651	21.590	8.50
241^0, 293^0	0.153	5.080	2.00
	.479	15.875	6.25

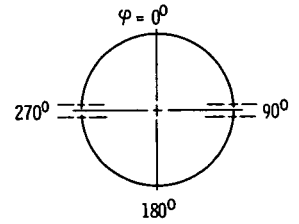

Looking upstream

Inside-surface temperatures

Angular position, φ	L/C	Distance from leading edge, L	
		cm	in.
5^0, 175^0	0.115	3.810	1.50
	.527	17.463	6.87
	.939	31.115	12.25
31^0, 149^0	0.115	3.810	1.50
	.871	28.887	11.37
59^0, 121^0	0.115	3.810	1.50
	.716	23.749	9.35
86^0	0.038	1.27	0.50
	.556	18.415	2.75

(f) Clamshell instrumentation.

Figure 9. - Concluded.

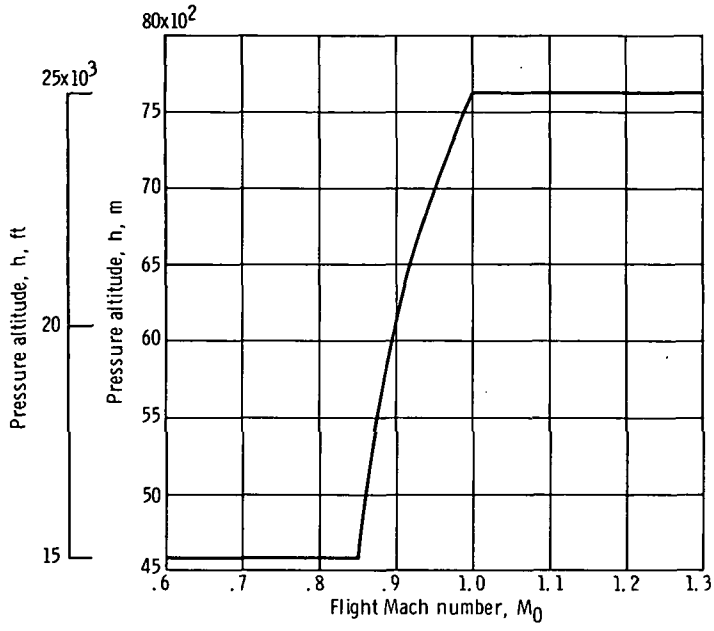

(a) Nominal flight test altitude - Mach number profile.

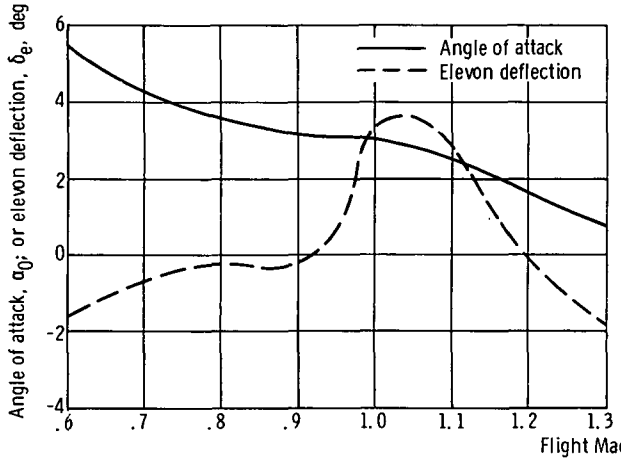

(b) Nominal angle of attack and elevon deflection with nacelles installed.

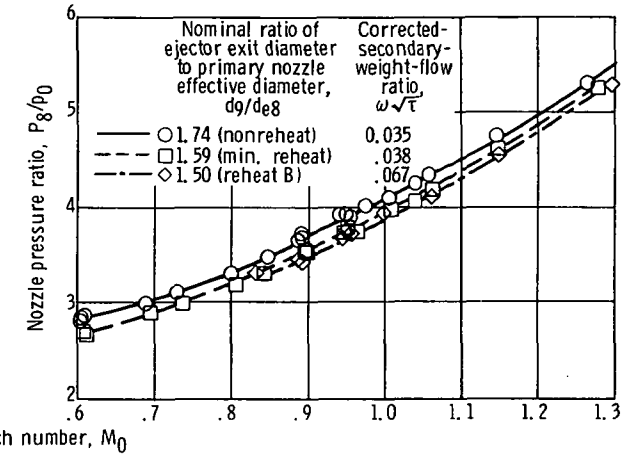

(c) Nozzle pressure ratio.

Figure 10. - Flight test conditions.

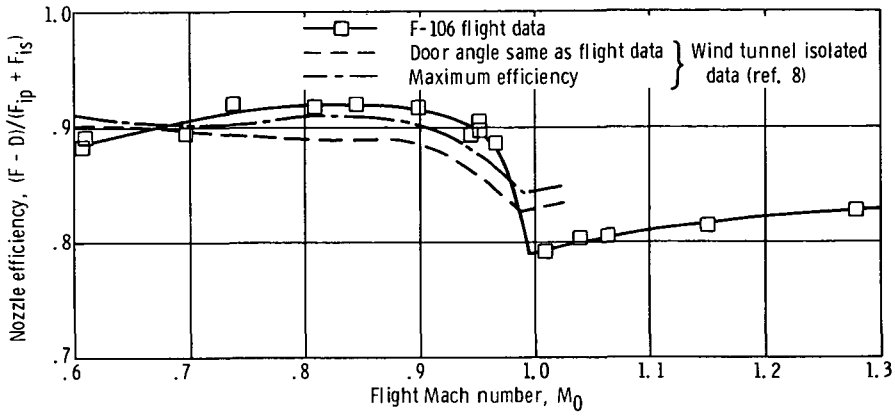

Figure 11. - Comparison of installed clamshell nozzle with isolated clamshell nozzle. Subsonic cruise configuration (minimum reheat; $d_9/d_{e8} = 1.59$, $\omega\sqrt{\bar{\tau}} = 0.04$).

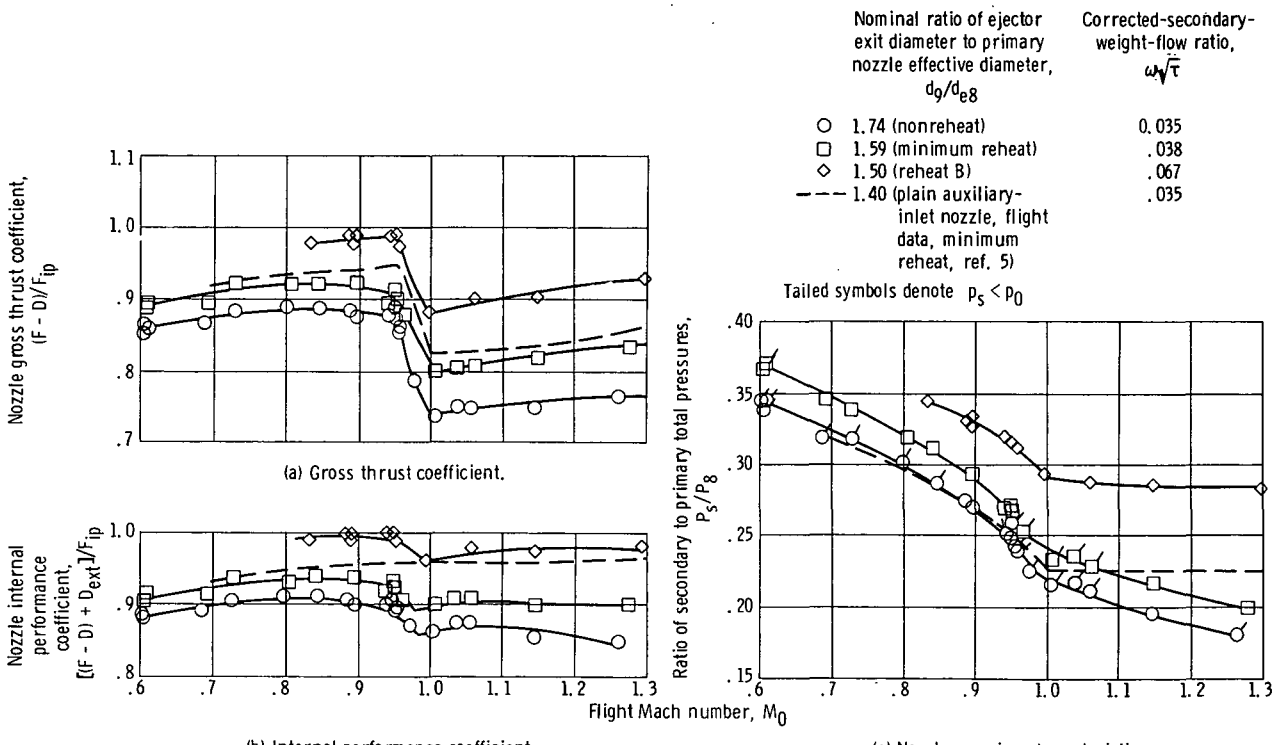

(a) Gross thrust coefficient.

(b) Internal performance coefficient.

(c) Nozzle pumping characteristics.

Figure 12. - Ejector nozzle performance characteristics and comparison with plain auxiliary-inlet nozzle.

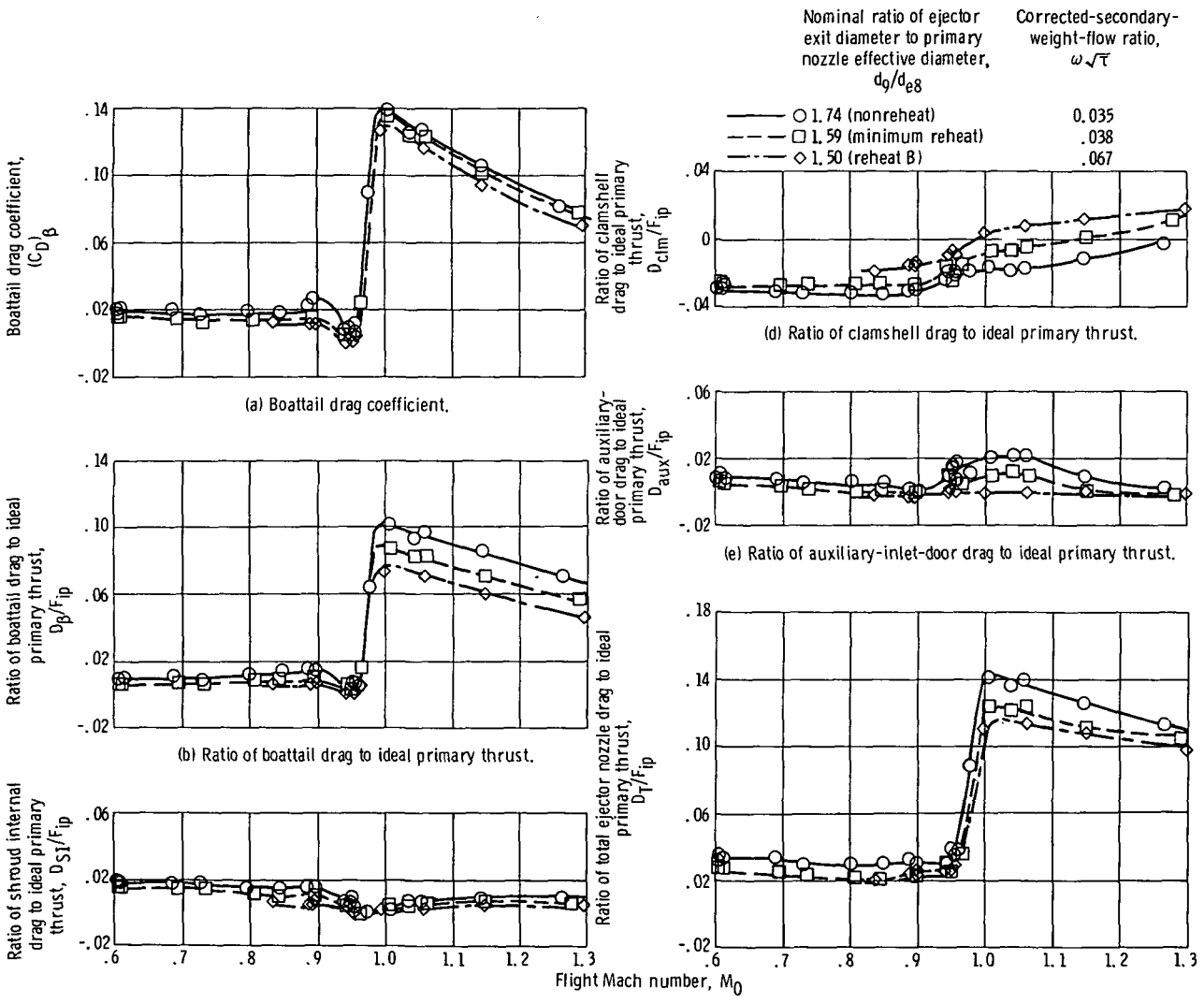

(a) Boattail drag coefficient.

(b) Ratio of boattail drag to ideal primary thrust.

(c) Ratio of shroud internal drag to ideal primary thrust.

(d) Ratio of clamshell drag to ideal primary thrust.

(e) Ratio of auxiliary-inlet-door drag to ideal primary thrust.

(f) Ratio of total ejector drag to ideal primary thrust.

Figure 13. - Component drag characteristics.

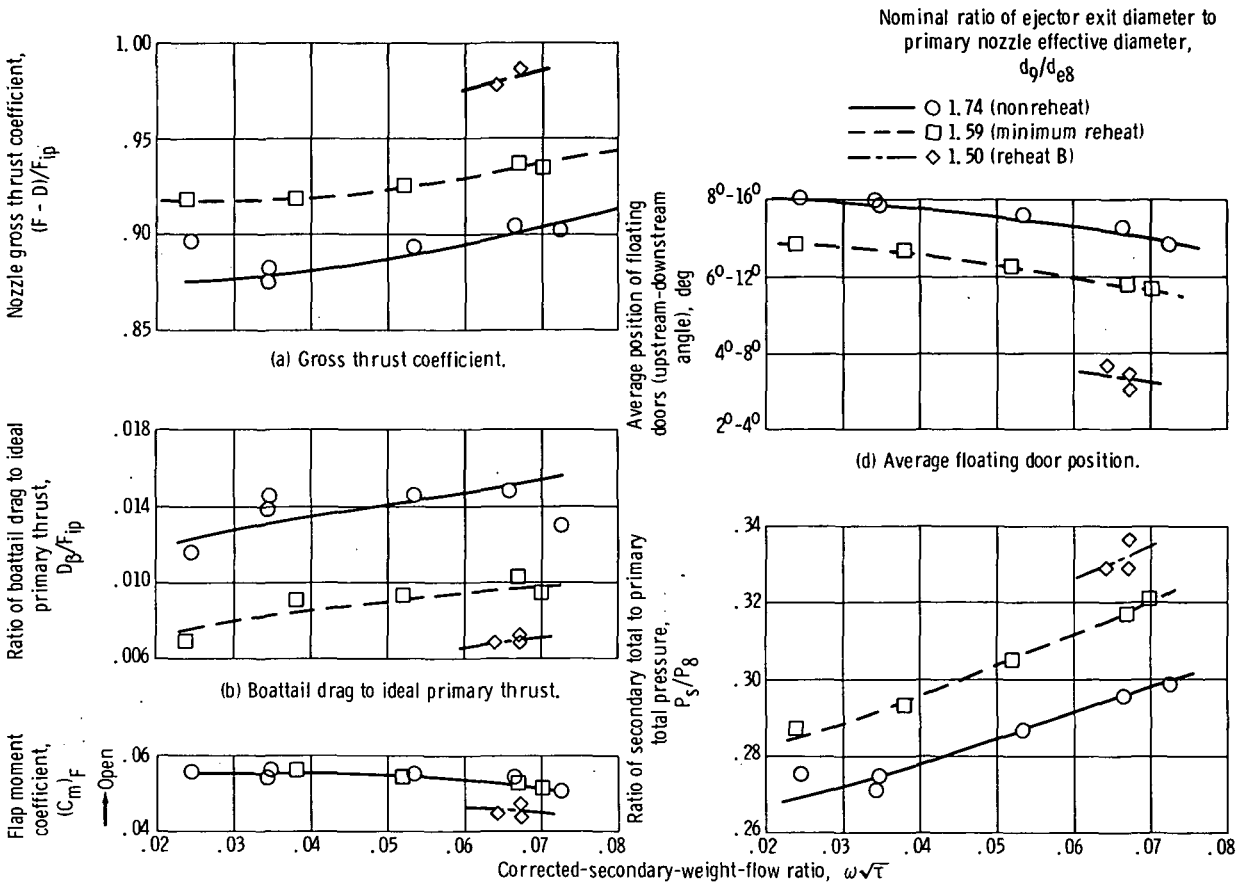

Figure 14. - Effect of corrected-secondary-weight-flow ratio on performance characteristics at Mach 0.9.

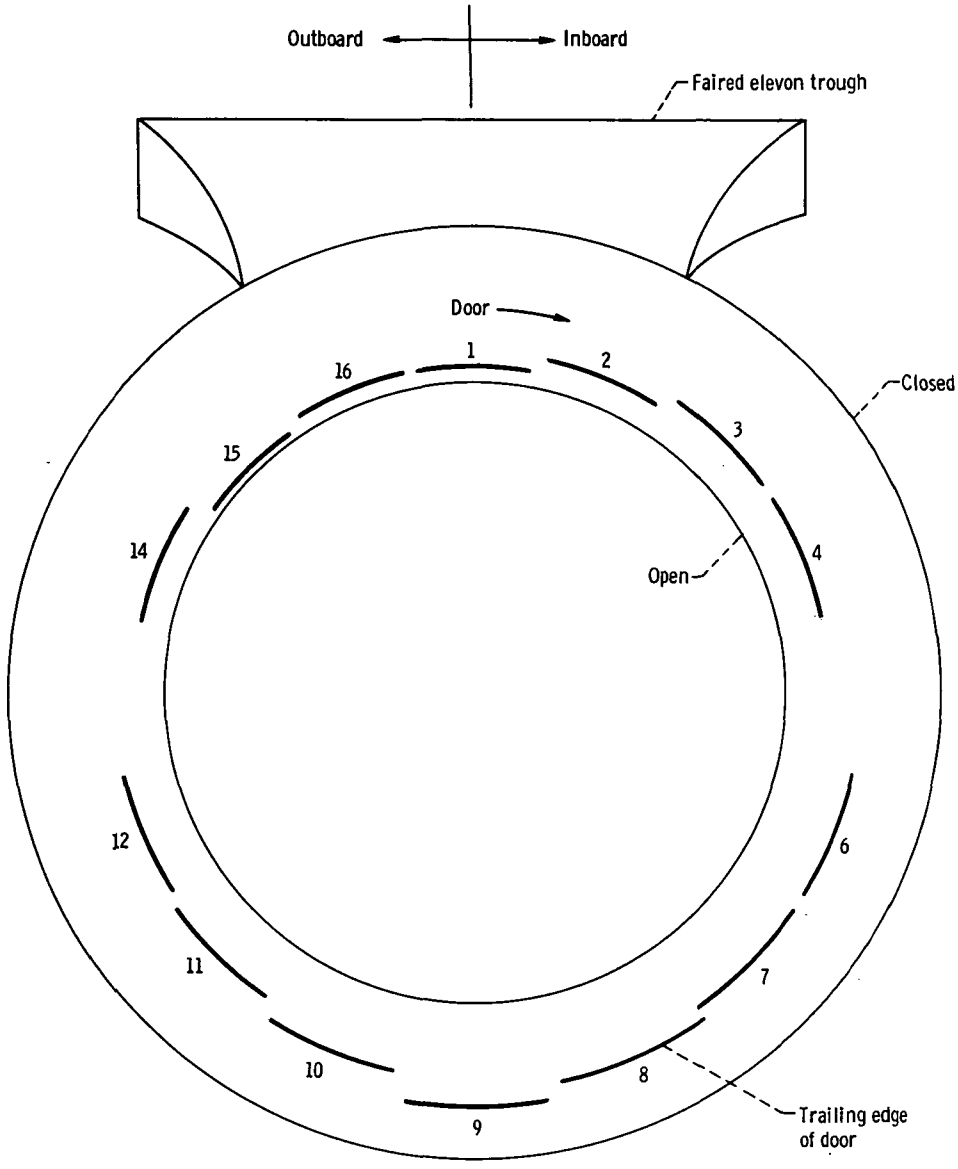

Figure 15. - Positions of synchronized floating doors. Mach number, 0.9; corrected-secondary-weight-flow ratio $\omega_s\sqrt{\theta}$, 0.038; nominal ratio of ejector exit diameter to primary nozzle effective diameter d_9/d_{e8}, 1.594 (minimum reheat); average door angle, 6.7°.

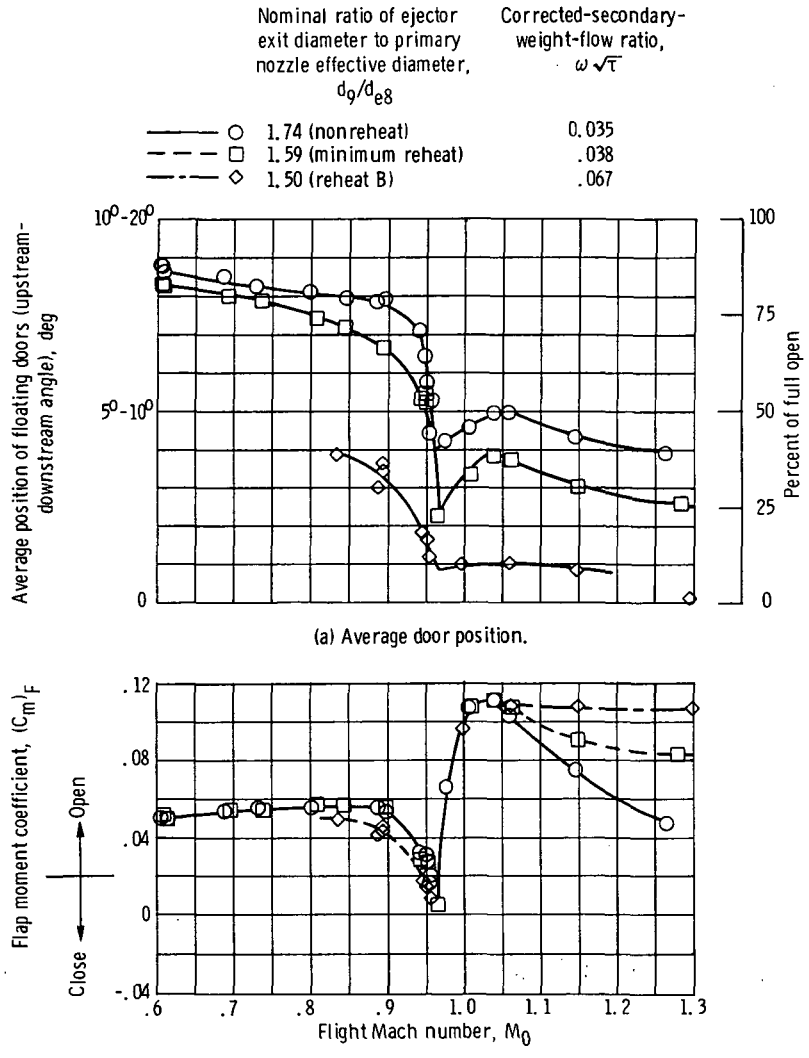

(a) Average door position.

(b) Flap moment coefficient.

Figure 16. - Flap moment and auxiliary-inlet-door floating characteristics.

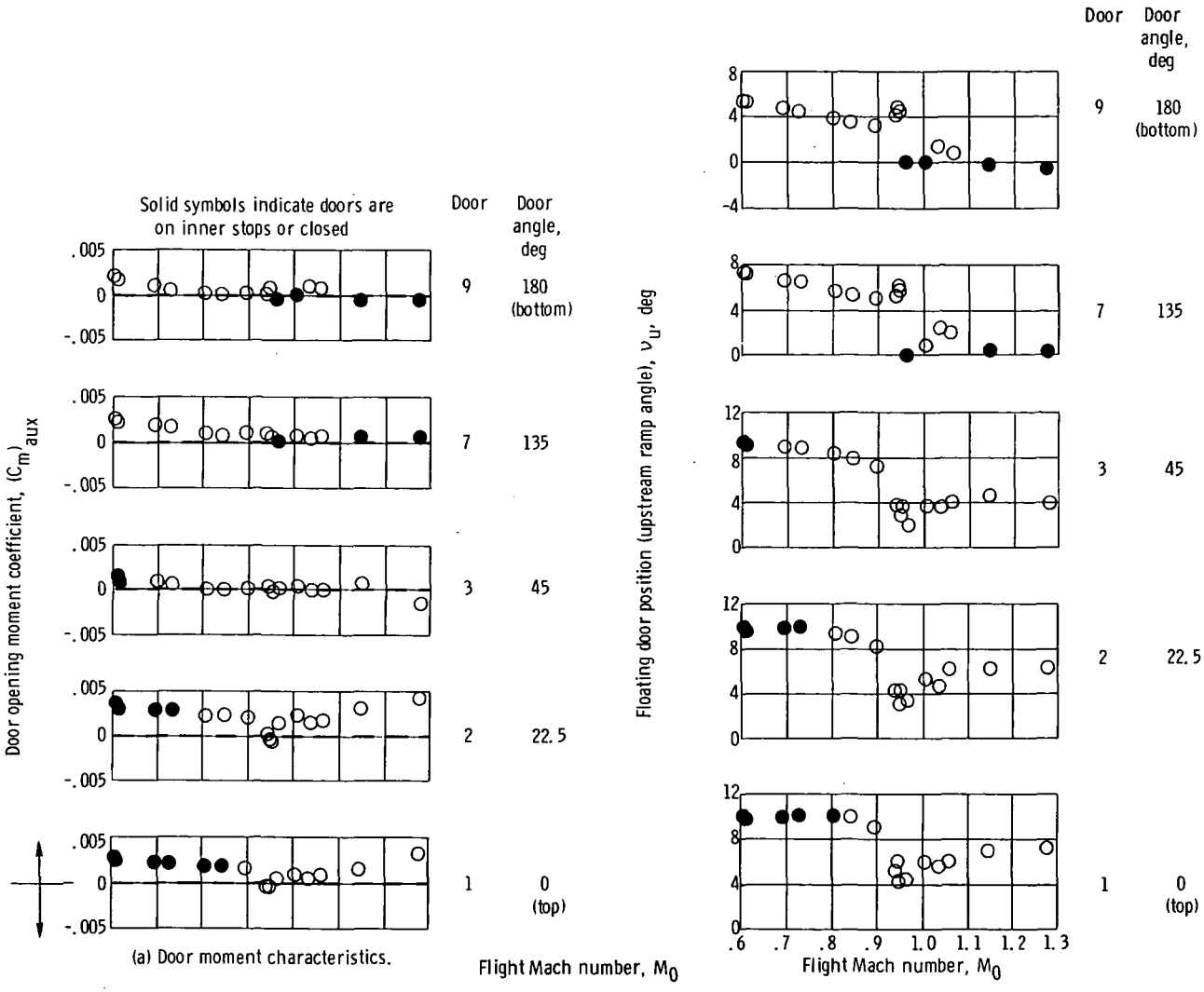

(a) Door moment characteristics.

(a) Door moment characteristics.

(b) Floating position characteristics.

Figure 17. - Selected blow-in door floating characteristics. Inboard doors; nominal ratio of ejector exit diameter to primary nozzle effective diameter d_9/d_{e8}, 1.59 (minimum reheat); corrected-secondary-weight-flow ratio $\omega\sqrt{\tau}$, 0.038.

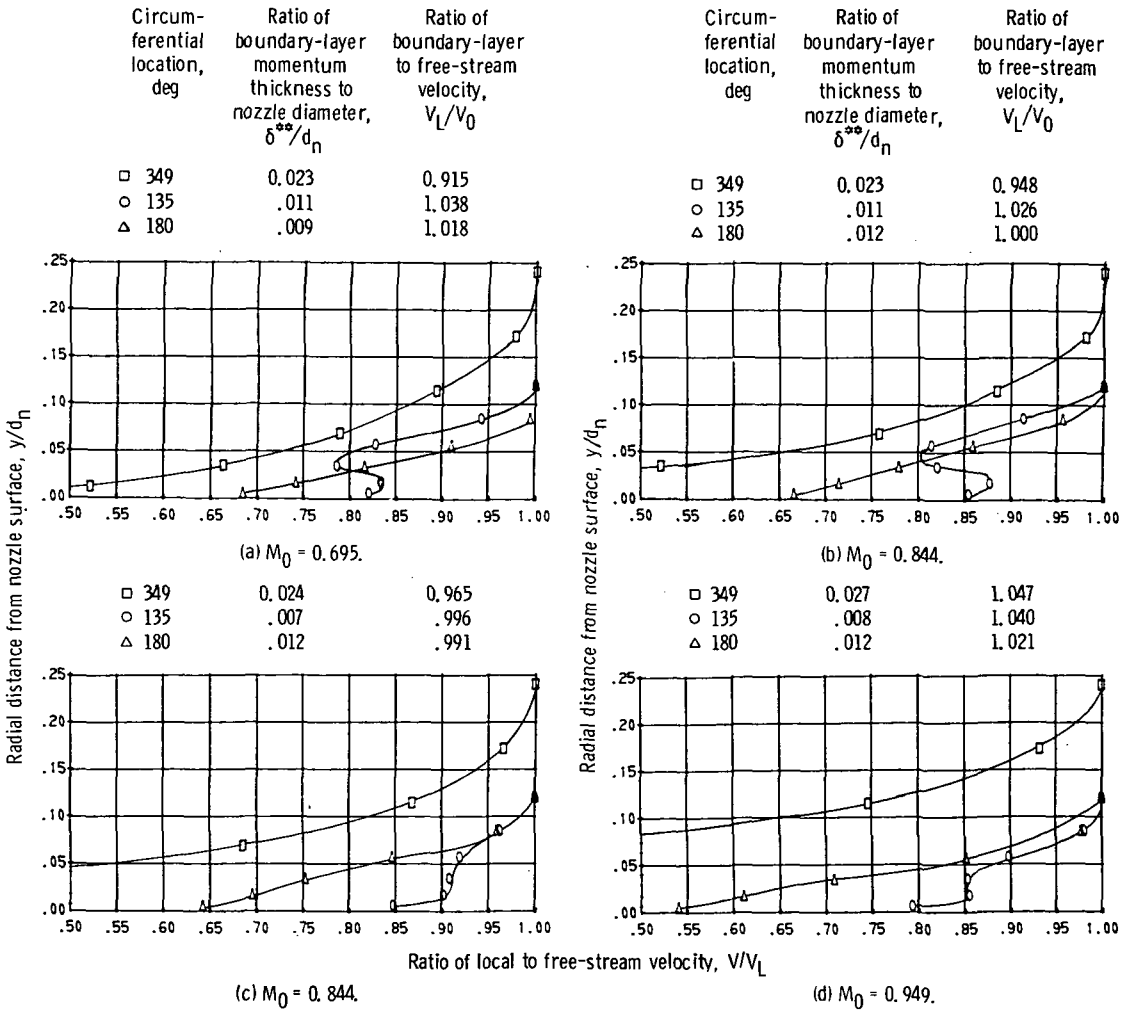

Figure 18. - Boundary-layer velocity profile upstream of auxiliary-inlet doors.

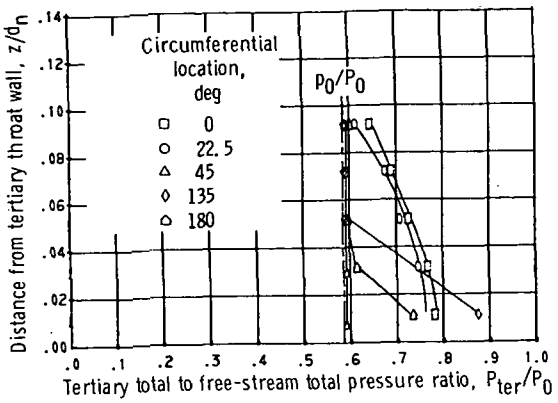

Figure 19. - Tertiary total-pressure recovery at door trailing edge. Free-stream Mach number, 0.897; nominal ratio of ejector exit diameter to primary nozzle effective diameter d_9/d_{e8}, 1.59 (minimum reheat); corrected-secondary-weight-flow ratio $\omega\sqrt{\tau}$, 0.038.

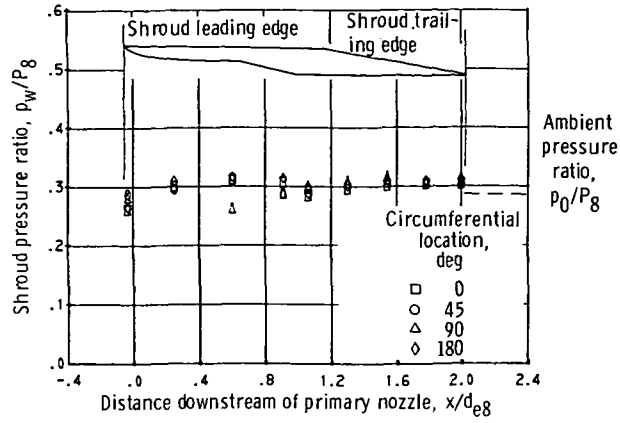

Figure 20. - Static-pressure distribution along internal surface of nozzle. Mach number, 0.9; nominal ratio of ejector exit diameter to primary nozzle effective diameter d_9/d_{e8}, 1.594 (minimum reheat); corrected-secondary-weight-flow ratio $\omega\sqrt{\tau}$, 0.038.

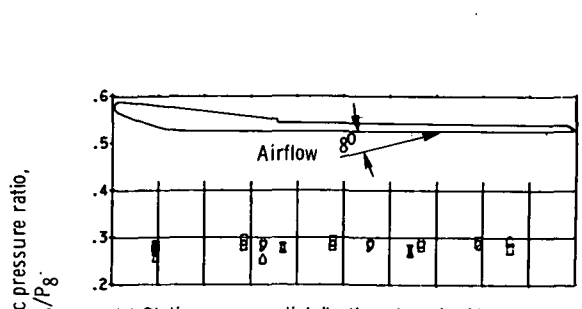

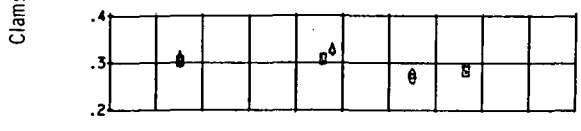

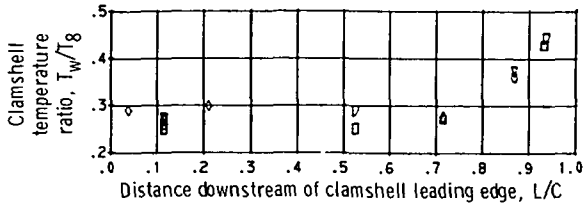

Clamshell static pressure ratio, p_w/P_8

Circumferential location, deg
5
31
59
86
94
121
149
175
194
220
247
293
320
346

(a) Static-pressure distribution along inside surface of clamshell.

(b) Static-pressure distribution along outside surface of clamshell.

Clamshell temperature ratio, T_w/T_8

Distance downstream of clamshell leading edge, L/C

(c) Temperature distribution along inside surface of clamshell.

Figure 21. - Clamshell static-pressure and surface-temperature distribution. Mach number, 0.9; nominal ratio of ejector exit diameter to primary nozzle effective diameter d_9/d_{e8}, 1.594 (minimum reheat); corrected-secondary-weight-flow ratio $\omega\sqrt{\tau}$, 0.038; gas temperature at nozzle throat T_8, 1259 K (2267° R).

NATIONAL AERONAUTICS AND SPACE ADMINISTRATION
WASHINGTON, D.C. 20546

OFFICIAL BUSINESS
PENALTY FOR PRIVATE USE $300

SPECIAL FOURTH-CLASS RATE
BOOK

POSTAGE AND FEES PAID
NATIONAL AERONAUTICS AND
SPACE ADMINISTRATION
451

U.S.MAIL

POSTMASTER: If Undeliverable (Section 158 Postal Manual) Do Not Return

"The aeronautical and space activities of the United States shall be conducted so as to contribute . . . to the expansion of human knowledge of phenomena in the atmosphere and space. The Administration shall provide for the widest practicable and appropriate dissemination of information concerning its activities and the results thereof."

—NATIONAL AERONAUTICS AND SPACE ACT OF 1958

NASA SCIENTIFIC AND TECHNICAL PUBLICATIONS

TECHNICAL REPORTS: Scientific and technical information considered important, complete, and a lasting contribution to existing knowledge.

TECHNICAL NOTES: Information less broad in scope but nevertheless of importance as a contribution to existing knowledge.

TECHNICAL MEMORANDUMS: Information receiving limited distribution because of preliminary data, security classification, or other reasons. Also includes conference proceedings with either limited or unlimited distribution.

CONTRACTOR REPORTS: Scientific and technical information generated under a NASA contract or grant and considered an important contribution to existing knowledge.

TECHNICAL TRANSLATIONS: Information published in a foreign language considered to merit NASA distribution in English.

SPECIAL PUBLICATIONS: Information derived from or of value to NASA activities. Publications include final reports of major projects, monographs, data compilations, handbooks, sourcebooks, and special bibliographies.

TECHNOLOGY UTILIZATION PUBLICATIONS: Information on technology used by NASA that may be of particular interest in commercial and other non-aerospace applications. Publications include Tech Briefs, Technology Utilization Reports and Technology Surveys.

Details on the availability of these publications may be obtained from:

SCIENTIFIC AND TECHNICAL INFORMATION OFFICE

NATIONAL AERONAUTICS AND SPACE ADMINISTRATION

Washington, D.C. 20546